NACA

RESEARCH MEMORANDUM

THE EFFECTS OF COMPRESSIBILITY ON THE PRESSURES ON A BODY

OF REVOLUTION AND ON THE AERODYNAMIC CHARACTERISTICS

OF A WING-NACELLE COMBINATION CONSISTING OF THE BODY

OF REVOLUTION MOUNTED ON A SWEPT-BACK WING

By Frederick W. Boltz and Benjamin H. Beam

Ames Aeronautical Laboratory
Moffett Field, Calif.

NATIONAL ADVISORY COMMITTEE
FOR AERONAUTICS
WASHINGTON
July 26, 1950

NATIONAL ADVISORY COMMITTEE FOR AERONAUTICS

RESEARCH MEMORANDUM

THE EFFECTS OF COMPRESSIBILITY ON THE PRESSURES ON A BODY

OF REVOLUTION AND ON THE AERODYNAMIC CHARACTERISTICS

OF A WING-NACELLE COMBINATION CONSISTING OF THE

BODY OF REVOLUTION MOUNTED ON A SWEPT-BACK WING

By Frederick W. Boltz and Benjamin H. Beam

SUMMARY

An investigation has been made of the effects of compressibility on the forces, on the pitching moments, and on the surface pressures on a wing-nacelle combination. The leading edge of the wing was swept back 37.25° and the nacelle was a body of revolution having a fineness ratio of 6.5. The effects of compressibility on the surface pressures and on the drag of a body of revolution similar to the nacelle were also determined.

Data are presented in this report for Mach numbers from 0.18 to 0.92 for the wing-nacelle combination and from 0.18 to 0.95 for the body of revolution, both for a Reynolds number of 2,000,000 based on the wing mean aerodynamic chord.

The effects of the nacelle on the lift and pitching-moment characteristics of the wing were found to be small. The pressure measurements indicated that local regions of high velocity occurring in the wing-nacelle junctures near the leading edge at low speeds persisted at high speeds. In spite of this interference effect, however, the drag-divergence Mach number of the wing-nacelle combination was only slightly lower than that of the plain wing. A critical Mach number based on local regions of high velocities in the wing-nacelle junctures is shown to be an unsatisfactory indication of the drag-divergence Mach number.

A method is presented for calculating the pressure coefficients over the body of revolution in compressible flow using the stream function and linear theory. Pressure coefficients calculated by this method are shown to agree well with the experimental pressure coefficients.

INTRODUCTION

An important objective of the current study of swept wings is the determination of the aerodynamic effects of nacelles and of external stores mounted on such wings. In previous investigations at subcritical speeds (references 1 and 2) local regions of high velocity have been observed at the junctures of a swept wing and a nacelle. Estimated critical Mach numbers based on the pressures in these regions of high velocity were found to be much lower than those based on the pressures on the swept wing without the nacelle. It became apparent, therefore, that further study was required to determine the degree to which interference from a nacelle may affect the force–divergence Mach number of a swept wing.

An investigation of the aerodynamic interference of a nacelle on a swept wing has been conducted in the Ames 12–foot pressure wind tunnel over a range of Mach numbers which included drag–divergence Mach numbers. The wing used in the investigation had 37.25° sweepback at the leading edge and had an aspect ratio of 6.04. The nacelle was simulated by a solid body of revolution having a fineness ratio of 6.5, and was mounted on the underside of the wing in such a way that the contour of the upper surface of the wing was changed only near the leading edge. The aerodynamic characteristics of the model wing without the nacelle have been reported in reference 3. In the present report the forces, pitching moments, and static pressures on the wing–nacelle combination are presented along with the drag and static–pressure measurements on an isolated body of revolution similar to the nacelle. A comparison of the static–pressure coefficients over the body of revolution with those predicted by linear theory has been included.

NOTATION

C_D drag coefficient based on wing plan–form area $\left(\dfrac{\text{drag}}{q_o S}\right)$

C_{D_F} drag coefficient based on frontal area of body of revolution

$$\left[\frac{\text{drag}}{q_o \,(\text{frontal area})}\right].$$

C_L lift coefficient $\left(\dfrac{\text{lift}}{q_o S}\right)$

C_m pitching–moment coefficient about the quarter point of the mean aerodynamic chord $\left(\dfrac{\text{pitching moment}}{q_o S \bar{c}}\right)$

L/D   ratio of lift to drag

M   Mach number $\left(\dfrac{V}{a}\right)$

M_{cr} critical Mach number, the free-stream Mach number at which sonic
       velocity is first attained

M_D drag-divergence Mach number, the free-stream Mach number at

       which $\left(\dfrac{\partial C_D}{\partial M_o}\right)_{C_L} = 0.10$

M_L lift-divergence Mach number, the free-stream Mach number at which
       the absolute value of lift coefficient at a constant angle of
       attack reaches a maximum

M_φ the free-stream Mach number at which the component of local Mach
       number normal to the isobar inclined at the angle φ equals
       unity at a specific point on the surface

P   pressure coefficient $\left(\dfrac{p-p_o}{q_o}\right)$

R_w Reynolds number based on wing chord $\left(\dfrac{\rho_o V_o \overline{c}}{\mu}\right)$

R_b Reynolds number based on body length $\left(\dfrac{\rho_o V_o l}{\mu}\right)$

S   semispan wing area, square feet

V   velocity, feet per second

a   speed of sound, feet per second

b/2   wing semispan normal to plane of symmetry, feet

c   local wing chord parallel to plane of symmetry, feet

$\overline{c}$ mean aerodynamic wing chord $\left(\dfrac{\int_o^{b/2} c^2 \, dy}{\int_o^{b/2} c \, dy}\right)$, feet

p   static pressure, pounds per square foot

q   dynamic pressure $\left(\frac{1}{2}\rho V^2\right)$, pounds per square foot

α   angle of attack, degrees

μ   coefficient of viscosity of air, slugs per foot–second

ρ   mass density of air, slugs per cubic foot

φ   local angle of sweep of isobars, degrees

Subscripts

o   free stream

u   uncorrected

MODELS AND APPARATUS

The semispan model wing upon which the nacelle was mounted was the model used in the swept–wing investigation reported in reference 3. The model represented one–half of a wing having the leading edge swept back 37.25°, an aspect ratio of 6.04, and a taper ratio of 0.5. No twist was built into the wing and the sections perpendicular to the quarter–chord line were the NACA 64_1–212, the coordinates of which are given in table I. The nacelle was a body of revolution having a fineness ratio of 6.5. From the nose of the nacelle to the maximum diameter the shape was that of a prolate spheroid, and from the maximum diameter to the tail the shape was that of a modified NACA 111 fuselage. The coordinates of the nacelle are given in table II. The nacelle was mounted on the under–side of the wing at 31 percent of the semispan as shown in figure 1. The wing–nacelle junctures were faired by the use of fillets behind the maximum diameter of the nacelle.

The model, a photograph of which is presented in figure 2(a), was built of laminated mahogany, secured to a steel spar. Chordwise rows of pressure orifices were situated at 15, 55, 73.3, and 91.7 percent of the semispan and at the wing–nacelle junctures and along the center lines of the upper and lower surfaces of the nacelle. The turntable, upon which the model was mounted, was directly connected to the force–measuring apparatus. Pressures were measured by means of multiple–tube manometers, the readings of which were recorded photographically.

The fineness ratio of the body of revolution was the same as that of the nacelle (6.5), but the ordinates differed slightly behind the 40–percent station as may be noted from table II. For the body, a short cylindrical

center section was used to join the prolate—spheroid forebody to the NACA 111 afterbody.

The body was constructed of laminated mahogany and was mounted on a 1—1/2—inch tube as shown in figure 2(b). Lengthwise rows of pressure orifices were located, as indicated in figure 1(a), along meridians 0°, 30°, 60°, 90°, 120°, 150°, 180°, and 270° from the top of the body. Also shown in figure 2(b) are the wake—survey rakes used in the determination of the drag. This survey equipment was removed for the measurements of surface pressures.

CORRECTIONS TO DATA

Tunnel—wall—interference corrections were evaluated by the method of reference 4, with the computations slightly modified to account for the effects of sweep. The following corrections were added to the data for the wing—nacelle combination:

$$\Delta\alpha = 0.489 \ C_L$$

$$\Delta C_D = 0.00754 \ C_L^2$$

No correction was applied to the angle of attack of the body of revolution.

The constriction corrections due to the presence of the tunnel walls were determined by the method of reference 5. While the method used is strictly applicable only to full—span models located centrally in the tunnel and does not allow for large angles of sweep, it has been used as the best available estimate of the constriction effects on the wing—nacelle combination. The magnitude of the corrections applied to the Mach number and to the dynamic pressure for the tests of the wing—nacelle combination is illustrated in the following table:

Corrected Mach number	Uncorrected Mach number	$\dfrac{\text{Corrected } q_o}{\text{Uncorrected } q_o}$
0.300	0.300	1.003
.400	.399	1.004
.500	.499	1.005
.600	.598	1.006
.700	.697	1.007
.800	.794	1.009
.850	.841	1.011
.900	.885	1.018
.920	.902	1.021

The constriction correction for the body of revolution due to the presence of the tunnel walls was also determined by the method of reference 5, and the magnitude of the corrections is illustrated in the following table:

Corrected Mach number	Uncorrected Mach number	$\dfrac{\text{Corrected } q_o}{\text{Uncorrected } q_o}$
0.800	0.799	1.001
.850	.849	1.002
.900	.897	1.003
.925	.921	1.004
.950	.943	1.007

The Mach number at which choking occurred in the tunnel test section with the model at 0° angle of attack was estimated to be 0.948 for the wing–nacelle combination and 0.960 for the body of revolution.

Corrections for the tare drag of the exposed surface of the turn-table were obtained with the model removed from the tunnel. The tare-drag coefficient was 0.0035 and was not affected by compressibility. The drag due to interference between the model and the turntable was not evaluated but was believed to have been small.

Drag data from the wake survey behind the body of revolution were evaluated by the method of reference 6. No attempt was made to evaluate the effect of body–sting interference on the body pressures.

TESTS

The static pressures on the wing–nacelle combination were measured simultaneously with the lift, drag, and pitching moment for Mach numbers from 0.18 to 0.92 at a constant Reynolds number of 2,000,000. The angle-of–attack range was from -8° to 20° at 0.18 Mach number and was reduced at higher Mach numbers because of model–strength and tunnel–power limitations.

Drag data for the body of revolution at 0° angle of attack were obtained by the wake–survey method for Mach numbers from 0.18 to 0.95 at a constant Reynolds number of 3,760,000 based on the length of the body or 2,000,000 based on the mean aerodynamic chord of the wing. Static pressures were measured through an angle–of–attack range of 0° to 8° for Mach numbers from 0.18 to 0.94 at the same Reynolds number.

RESULTS AND DISCUSSION

Aerodynamic interference between the nacelle and the swept wing is evaluated in this report by considering the pressures and forces on each separately and comparing them with those on the wing-nacelle combination. The forces, moments, and static pressures on the isolated wing have been reported in reference 3. Drag data and static pressures for the body of revolution are included in the present report and will be discussed first.

Body of Revolution

The variation in drag coefficient with Mach number for the body of revolution at 0° angle of attack is presented in figure 3. In the range of Mach numbers from 0.18 to 0.92 the change in drag coefficient with Mach number was small. The critical Mach number, determined from static-pressure data, was approximately 0.90.

In figures 4 through 8, the lengthwise distribution of pressure coefficient along several meridians of the body is presented for various Mach numbers at angles of attack from 0° to 8°. The location of the meridians indicated in these figures is shown in figure 1. The experimentally determined pressure coefficients have been compared with the calculated pressure coefficients in figures 9, 10, and 11.

To calculate the pressure coefficients over the body in incompressible flow, the source-sink distribution for the body was used to obtain the stream function from which the velocity components were derived. The Prandtl-Glauert method was used to extend the calculation to compressible flow. (See reference 7.) A detailed explanation of the method of calculation for both the incompressible-flow solution and the linearized compressible-flow solution is given in Appendix A.

In figure 9, the lengthwise distribution of pressure coefficient calculated by this method is compared with the experimental data for Mach numbers of 0.18 and 0.90 and 0° angle of attack. The incompressible-flow calculation (i.e., for a Mach number of zero) is shown to agree well with the experimental data at a Mach number of 0.18. The difference between the pressure coefficients calculated by the incompressible-flow theory and the linearized compressible-flow theory for a Mach number of zero illustrates the order of magnitude of the error introduced in linearizing the equations of motion. At a Mach number of 0.90 the calculated pressure distribution agrees well with that obtained experimentally.

In figure 10, the pressure coefficients calculated by the linear theory at the minimum-pressure point for 0° angle of attack are compared with the experimental pressure coefficients at the same point throughout the subsonic Mach number range. The variation of the experimental

pressure coefficients with Mach number is approximately the same as that predicted by linear theory, although the experimental pressure coefficients are slightly more negative than the calculated pressure coefficients at all Mach numbers.

In figure 11, the calculated pressure coefficients at the 26.9-percent station on the upper and lower meridians of the body in inclined flow are shown compared with the experimental values for the same locations through the subsonic Mach number range for angles of attack of 2°, 4°, 6°, and 8°. The method of calculation is explained in Appendix B.[1] The good agreement between the calculated and the experimental pressure coefficients is evidence that the linear theory can be applied to the prediction of pressure changes with Mach number for a body of revolution in an inclined field of flow. The change of pressure coefficient with Mach number is shown to be practically independent of the angle of attack.

Wing—Nacelle Combination

Force and moment characteristics.— In figure 12 the lift, drag, and pitching—moment characteristics of the wing—nacelle combination are shown compared with those of the wing alone for Mach numbers from 0.18 to 0.92 at a Reynolds number of 2,000,000. Data for the wing alone have been presented in reference 3. The variation of the lift and pitching—moment coefficients with Mach number is shown in figure 13 and the variation of the lift—curve slope and aerodynamic center is shown in figure 14.

Addition of the nacelle to the plain wing had only small effects on the lift—curve slope and on the Mach number for lift divergence, but increased the angle of attack for zero lift by approximately $1/2^o$. At zero lift, the aerodynamic center of the wing—nacelle combination was ahead of the aerodynamic center of the wing alone by an amount varying from 0 to 3 percent of the mean aerodynamic chord for Mach numbers less than 0.90. For both the plain wing and the wing—nacelle combination, the aerodynamic center moved rearward as the Mach number was increased above 0.80. Addition of the nacelle resulted in smaller negative values of the pitching moment for zero lift at the higher Mach numbers.

The variation of drag coefficient with Mach number is presented in figure 15. At lift coefficients of 0.3 and less, the drag of the wing—nacelle combination began to increase at a somewhat lower Mach number than that at which the drag increased for the plain wing. At a lift coefficient of 0.4 this premature drag increase did not occur. The drag-divergence Mach number for each lift coefficient has been noted in

---

[1]A recent paper by H. Julian Allen (reference 8) gives another method for calculating the pressure coefficients due to inclined flow.

figure 15. It appears that the addition of the nacelle caused very little reduction in the drag-divergence Mach number.

The variation of maximum L/D, of lift coefficient for maximum L/D, and of minimum drag coefficient with Mach number are presented in figure 16. As would be expected, the addition of the nacelle caused a reduction in maximum L/D as a result of the increased drag due to the nacelle. The lift coefficient for maximum L/D was only slightly affected by the addition of the nacelle to the wing.

Pressure distribution.— The distribution of static-pressure coefficient over the wing-nacelle combination is presented in the form of isobar diagrams in figures 17, 18, and 19 for a range of Mach numbers and for angles of attack of 0°, 2°, and 4°. In figure 20, portions of these data are compared with similar data for the plain wing from reference 3. The crest line (defined as the locus of points at which the wing surface is tangent to the direction of the undisturbed air stream) is indicated on all the isobar diagrams for use as a reference line in estimating the effects of the changing pressure distribution on the drag. To show more clearly the effect of compressibility on the pressures in the wing-nacelle junctures, the distributions of pressure coefficient in each of the four junctures are compared in figure 21 at several Mach numbers for angles of attack of 0°, 2°, and 4°.

Examination of figures 17, 18, and 19 reveals that a region of high negative pressure coefficients existed near the leading edge at the inner juncture of the wing and the nacelle. On the upper surface the extent of the region was small, even at Mach numbers beyond that for drag divergence. From figure 20 it may be noted that the pressures over the remainder of the upper surface of the wing-nacelle combination were about the same as for the plain wing. On the lower surface of the wing-nacelle combination, interference caused a region of high velocities in the inner juncture and influenced the pressure distribution over much of the area between the nacelle and the plane of symmetry. The change in the pressure distribution was such as to reduce the sweep of the isobars and thus to reduce the effectiveness of sweepback of the wing.

In figure 20(a), the chordwise distribution of pressure coefficient over the upper and lower surfaces of the wing-nacelle combination at a station half way between the nacelle and the wing root is compared with that for the wing without the nacelle at 0° angle of attack. The addition of the nacelle resulted in a forward movement of the point of minimum pressure on the upper surface and in a slight increase in the sweep of the isobars, but caused only a small increase in maximum surface velocity at this station. On the lower surface near the nacelle, the presence of the nacelle caused a large decrease in minimum pressure as well as a reduction in sweep of the isobars, both of which decreased the free-stream Mach number at which a shock wave could form on the wing. The premature drag increase of the wing-nacelle combination with increasing Mach number at low lift coefficients, noted with reference to figure 15, was probably the result of this shock-wave formation.

From figure 20(b), it is noted that at 4° angle of attack the veloc—
ities on the lower surface of the wing—nacelle combination were much lower
than on the upper surface. Thus, shock waves must have occurred first on
the upper surface at this angle of attack. The drag data of figure 15
showed no premature drag increase at a lift coefficient of 0.4, which
corresponds to approximately 4° angle of attack, in spite of the local
region of high velocity at the inner wing—nacelle juncture on the upper
surface near the leading edge.

In figure 21, it may be seen that at 0° angle of attack there was
little change in the type of chordwise distribution of pressure coeffi—
cient in the wing—nacelle junctures up to a Mach number of 0.85. However,
as the Mach number was increased to 0.90, there was a rearward movement
of the region of low pressure in all but the lower outer juncture. At
angles of attack of 2° and 4°, this rearward movement of low pressure,
resulting from the development of supersonic flow, began at a Mach number
between 0.80 and 0.85.

Critical and drag—divergence Mach numbers.— In a detailed analysis
of the forces and pressures on this swept wing, it was shown in refer—
ence 3 that the drag—divergence Mach number was only slightly greater than
the Mach number at which critical flow conditions had developed along the
crest of the entire wing. A critical flow condition was considered to
occur when the component of local Mach number normal to the isobars became
equal to unity. The free—stream Mach number for the attainment of the local
critical—flow condition has been denoted by the symbol M_φ to distinguish
it from the critical Mach number M_{cr}. When the sweep of the isobars is
zero, M_φ is obviously equal to M_{cr}.

Figure 22 is presented to show the relation between the drag increase
and the attainment of critical flow conditions at several points on the
wing—nacelle combination. In this figure, the pressure coefficients at
the crest of the upper surface at several spanwise stations, the minimum
pressure coefficients in the upper and lower wing—nacelle junctures, and
the total drag coefficient of the wing—nacelle combination are shown as
functions of Mach number. The dashed curves represent the variation with
Mach number of the pressure coefficients corresponding to the critical
flow condition for sweep angles of 0° and 35°. The intersections of the
solid and dashed curves define a range of Mach numbers within which criti—
cal flow conditions were attained. An inspection of figure 22 discloses
that, for angles of attack of 0° and 2°, the drag coefficient started to
increase rapidly at about the Mach number at which the critical flow condi—
tion was attained along the crest of the upper surface. Moreover, it is
apparent that the local velocities in the junctures reached the sonic value
at Mach numbers well below that for drag divergence.

The relation of the drag—divergence Mach number to the critical Mach
number based on minimum pressures in the junctures is illustrated in
figure 23. In this figure, the drag—divergence Mach number of the wing—
nacelle combination, that of the plain wing, and the critical Mach numbers

of the upper and lower wing-nacelle junctures are shown as functions of lift coefficient. It is apparent that critical Mach numbers based on localized areas of low pressure do not provide a satisfactory estimate of the drag-divergence Mach number. In the case of the present wing-nacelle combination, the drag-divergence Mach number almost equaled that of the plain wing.

CONCLUSIONS

Tests have been conducted at Mach numbers up to 0.92 and at a constant Reynolds number of 2,000,000 to determine the effects of mounting a nacelle of fineness ratio 6.5 on a wing having the leading edge swept back 37.25°. The results of these tests may be summarized as follows:

1. The lift and pitching-moment characteristics of the wing were only slightly changed by the addition of the nacelle.

2. At lift coefficients less than 0.3, the nacelle caused the drag to increase at a somewhat lower Mach number than that at which the wing-alone drag began to increase. At a lift coefficient of 0.4, this premature drag increase did not occur. In spite of the earlier drag rise, the drag-divergence Mach number (defined as the Mach number at which $\partial C_D/\partial M_o = 0.10$ at constant lift coefficient) was reduced no more than 0.01 by the addition of the nacelle.

3. The upper-surface velocities on the wing-nacelle combination were about the same as for the plain wing, except for a small region of high velocity at the inner juncture near the leading edge. On the lower surface there was considerable distortion of the velocity distribution, which apparently caused the earlier drag rise at the lower lift coefficients.

4. The critical Mach number based on the pressures in the wing-nacelle junctures did not furnish a satisfactory estimate of the drag-divergence Mach number.

From the results of tests at Mach numbers up to 0.95 of an isolated body of revolution similar to the nacelle, it was found that:

1. The drag coefficient of the body at 0° angle of attack varied only a small amount up to a Mach number of approximately 0.92.

2. Good agreement existed between the experimental values of pressure coefficient and those calculated by theory.

Ames Aeronautical Laboratory,
    National Advisory Committee for Aeronautics,
        Moffett Field, Calif.

APPENDIX A

CALCULATION OF THE FLOW ABOUT THE BODY
OF REVOLUTION IN AN AXIAL—FLOW FIELD

The body of revolution used in this investigation was formed by com-
bining parts of two other bodies for which the source—sink distributions
were known: a prolate spheroid and a modified NACA 111 body. This appen-
dix will show the method used to calculate the incompressible flow about
the prolate—spheroid forebody and the modified NACA 111 afterbody using
their source—sink distributions. The method will then be extended to
compressible flow by linear theory.

As shown in reference 9, the source strength for the prolate
spheroid varies linearly from a maximum at the forward focus to zero at
the maximum thickness. In reference 10, the sink strength for the
NACA 111 body is shown to increase linearly from zero at 40 percent of
the length to a maximum at 70 percent, and then to decrease linearly to
zero at the tail. It is assumed that the source—sink distribution for
the test body of revolution is that of a prolate spheroid for the forebody
and that of the NACA 111 for the afterbody. This assumption is believed
justified, since for bodies of the fineness ratio being considered the
velocities over the forward portion of the body are practically unaffected
by small changes in shape of the afterbody, and velocities over the
afterbody are little affected by small changes in the forebody. Further-
more, the change in fineness ratio from 5 for the NACA 111 body to 6.5 for
the test body would affect the sink strength with respect to the free
stream, but would not materially affect its distribution.

The condition that produces a closed body of unit length from an
arrangement of sources and sinks along a ξ axis, where $f(\xi)$ is the
source strength per unit length, is

$$\int_0^1 f(\xi)\, d\xi = 0 \tag{A1}$$

as explained in reference 11. By applying the condition

$$\left.\begin{array}{l} \displaystyle\int_0^{0.4000} f(\xi)\, d\xi = 1 \\[2em] \displaystyle\int_{0.4000}^1 f(\xi)\, d\xi = -1 \end{array}\right\} \tag{A2}$$

the expression for $f(\xi)$ was determined as follows:

$f(\xi) = 0$ from $\xi = 0$ to $\xi = e$

$f(\xi) = 5.305 - 14.07(\xi - e)$ " $\xi = e$ to $\xi = 0.3847$

$f(\xi) = 0$ " $\xi = 0.3847$ to $\xi = 0.4000$

$f(\xi) = -11.11 (\xi - 0.4000)$ " $\xi = 0.4000$ to $\xi = 0.7000$

$f(\xi) = -3.333 + 11.11(\xi - 0.7000)$ " $\xi = 0.7000$ to $\xi = 1.0000$

where e is the distance from the nose to the focus of the prolate-spheroid forebody, defined by

$$e = (0.3847) - \sqrt{(0.3847)^2 - \left(\frac{\text{maximum thickness}}{2}\right)^2}$$

The ξ axis along which the sources lie is now assumed to be coincident with the x axis. The stream function from the source-sink distribution can then be regarded as the difference in the amount of fluid flowing inside a circle of radius r, the plane of which is normal to the x axis and the center of which is on the x axis, and the amount of fluid delivered by the source-sink distribution upstream of x. Thus, where ψ_1 is the stream function of the source-sink distribution (reference 11)

$$\psi_1 = -\frac{1}{2} \int_0^1 f(\xi) \left(1 + \frac{x-\xi}{b}\right) d\xi \qquad (A3)$$

in which

$$b = \sqrt{(x-\xi)^2 + r^2}$$

The stream function, ψ_2, due to the superimposed flow parallel to the x axis is

$$\psi_2 = \pi r^2 U_0 \qquad (A4)$$

where U_0 is the free-stream velocity. The total stream function, ψ, thus becomes

$$\psi = \psi_1 + \psi_2 = \pi r^2 U_0 - \frac{1}{2} \int_0^1 f(\xi) \left(1 + \frac{x-\xi}{b}\right) d\xi \qquad (A5)$$

Equating the total stream function to zero results in the equation of the
surface of the body. It is apparent that for a given $f(\xi)$ different
values of U_O will produce a family of bodies of different fineness
ratios. Letting ψ equal zero and solving for the value of U_O that
corresponds to the fineness ratio of the test body gives

$$U_O = \frac{1}{2\pi r^2} \int_O^1 f(\xi) \left(1 + \frac{x-\xi}{b}\right) d\xi \qquad (A6)$$

Any values of x and r that correspond to points on the surface of the
body (except at the nose and tail) can be used to evaluate U_O. The
velocities of the flow due to the source—sink distribution, parallel to
the x axis, Δu, and normal to the x axis, Δv, are then (refer-
ence 11)

$$\Delta u = \frac{1}{2\pi r} \frac{\partial \psi_1}{\partial r} \qquad (A7)$$

$$\Delta v = \frac{1}{2\pi r} \frac{\partial \psi_1}{\partial x} \qquad (A8)$$

and the pressure coefficient for the incompressible flow becomes

$$P = -\left[2 \frac{\Delta u}{U_O} + \left(\frac{\Delta u}{U_O}\right)^2 + \left(\frac{\Delta v}{U_O}\right)^2\right] \qquad (A9)$$

The result of this equation is shown graphically in figure 9 as the
incompressible—flow solution.

The equations developed for incompressible flow can now be extended
to compressible flow. In the appendix of reference 7, it is shown that
a first—order approximation of the subsonic compressible flow about a
three—dimensional body can be obtained in three steps. This method,
originally developed by Göthert, can be applied to the body of revolution
in the following manner:

1. The radial coordinates of all points on the surface of the body
are contracted by a factor $\beta = \sqrt{1 - M_O^2}$ where M_O is the free—stream
Mach number. (In reference 7 the x coordinates are expanded in place
of contracting the radial coordinates. The two procedures lead to the
same result, but expanding the longitudinal coordinates involves computing
difficulties for bodies of unit length.)

2. The free—stream velocity $U_O{}'$ and the velocities due to the
source—sink distribution, $\Delta u'$ and $\Delta v'$, are calculated as if the con-
tracted body were in incompressible flow.

3. The values of U_o, Δu, and Δv in the compressible-flow field of the original uncontracted body are found by the following equations:

$$U_o = U_o{}' \tag{A10}$$

$$\Delta u = \frac{1}{\beta^2}\, \Delta u' \tag{A11}$$

$$\Delta v = \frac{1}{\beta}\, \Delta v' \tag{A12}$$

Thus, in the present case, the source-sink distribution was retained as in the incompressible flow, but the evaluation of the velocity components was made for a body the fineness ratio of which was $1/\beta$ times that of the test body. These velocities were then multiplied by the factors in step 3 above.

The pressure coefficients in the compressible flow cannot be computed with the same accuracy as in the incompressible flow, because the steps above were developed from a linearized equation of motion and boundary condition. (See reference 7.) To linearize the equation it was necessary to neglect all values of $\Delta u/U_o$ and $\Delta v/U_o$ that were of higher degree than the first and all cross products of these quantities (a procedure first used by Prandtl and Glauert). This leaves the expression for the pressure coefficient calculated for compressible flow by linear theory as

$$P = -2\,\frac{\Delta u}{U_o} \tag{A13}$$

The result of this equation is shown graphically in figures 9 and 10.

The velocity components for this body in compressible flow, as evaluated by the methods explained in the foregoing paragraphs, are given in equations (A14), (A15), and (A16). The incompressible velocity components can be obtained by considering $\beta = 1$.

$$U_o = \frac{1}{\pi\beta^2 r^2}\left\{-\frac{b_e}{\epsilon} + \frac{1}{2\epsilon^2}\left[b_e(x - 0.3847 + \epsilon) - b_f(x - 0.3847) - \right.\right.$$

$$\left. \beta^2 r^2\, \ln\left(\frac{x-0.3847 + b_f}{x-0.3847 + b_e + \epsilon}\right)\right] + 2.777\left[b_g(0.4000+x) - 2b_h(0.7000+x) + \right.$$

$$0.8000(b_h-b_g) - 2(b_1-b_h) + b_1(x+1.0000) + \beta^2 r^2 \ln \frac{(x-1.0000+b_1)(x-0.4000+b_g)}{(x-0.7000+b_h)^2}$$

$$\tag{A14}$$

$$\Delta u = \frac{1}{2\pi\beta^2} \left\{ -\frac{1}{\epsilon b_e} + \frac{1}{2\epsilon^2} \left[\frac{(x-0.3847+\epsilon)}{b_e} - \frac{(x-0.3847)}{b_f} - 2ln\left(\frac{x-0.3847+b_f}{x-0.3847+\epsilon+b_e}\right) - \right. \right.$$

$$\left. \beta^2 r^2 \left(\frac{1}{b_f(x-0.3847+b_f)} - \frac{1}{b_e(x-0.3847+\epsilon+b_e)}\right) \right] +$$

$$2.777 \left[\frac{(0.4000+x)}{b_g} - \frac{2(0.7000+x)}{b_h} + 0.8000\left(\frac{1}{b_h} - \frac{1}{b_g}\right) - 2\left(\frac{1}{b_1} - \frac{1}{b_h}\right) + \right.$$

$$\frac{(x+1.0000)}{b_1} + 2ln\frac{(x-1.0000+b_1)(x-0.4000+b_g)}{(x-0.7000+b_h)^2} - \beta^2 r^2 \left(\frac{2}{b_h(x-0.7000+b_h)} - \right.$$

$$\left.\left.\left. \frac{1}{b_g(x-0.7000+b_g)} - \frac{1}{b_1(x-1.0000+b_1)}\right)\right]\right\} \qquad \text{(A15)}$$

$$\Delta v = -\frac{1}{2\pi\beta r} \left\{ -\frac{(x-0.3847+\epsilon)}{\epsilon b_e} + \frac{1}{2\epsilon^2}\left[\frac{(x-0.3847+\epsilon)^2}{b_e} - \frac{(x-0.3847)^2}{b_f} + b_e - b_f - \right.\right.$$

$$\left.\beta^2 r^2\left(\frac{1}{b_f} - \frac{1}{b_e}\right)\right] + 2.777\left[\frac{x^2-0.1600}{b_g} - \frac{2(x^2-0.4900)}{b_h} + b_g - 2b_h + \right.$$

$$0.8000\left(\frac{x-0.7000}{b_h} - \frac{x-0.4000}{b_g}\right) - 2\left(\frac{x-1.0000}{b_1} - \frac{x-0.7000}{b_h}\right) +$$

$$\left.\left.\frac{(x^2-1.0000)}{b_1} + b_1 + \beta^2 r^2\left(\frac{1}{b_1} + \frac{1}{b_g} - \frac{2}{b_h}\right)\right]\right\} \qquad \text{(A16)}$$

where

$$\beta = \sqrt{1 - M_o{}^2}$$

$$\epsilon = \sqrt{0.1479 - 0.00591\beta^2}$$

$$b_e = \sqrt{(x - 0.3847 + \epsilon)^2 + \beta^2 r^2}$$

$$b_f = \sqrt{(x - 0.3847)^2 + \beta^2 r^2}$$

$$b_g = \sqrt{(x - 0.4000)^2 + \beta^2 r^2}$$

$$b_h = \sqrt{(x - 0.7000)^2 + \beta^2 r^2}$$

$$b_l = \sqrt{(x - 1.0000)^2 + \beta^2 r^2}$$

APPENDIX B

CALCULATION OF THE FLOW ABOUT THE BODY OF .
REVOLUTION IN AN INCLINED FLOW FIELD

The velocities along the upper and lower meridians of the body of
revolution in inclined flow can be calculated for incompressible flow
using the theory of airships. In reference 12, an equation for transverse
force is developed from consideration of the flow about ellipsoids of
revolution.

$$\Delta F_t = q_0 \pi \, r \, \sin 2\varphi \, \sin 2\alpha \qquad (B1)$$

where

ΔF_t transverse force per unit length

x, r body coordinates

q_0 free—stream dynamic pressure

φ $\tan^{-1} \dfrac{dr}{dx}$

α angle of attack

This simple formula has been shown by comparison with experimental data
to give the general distribution and magnitude of the transverse force with
a high degree of accuracy.

Since

$$\varphi = \tan^{-1} \frac{dr}{dx}$$

$$\sin 2\varphi = \frac{2 \dfrac{dr}{dx}}{1 + \left(\dfrac{dr}{dx} \right)^2}$$

And thus

$$\Delta F_t = \frac{2 q_0 \pi \, r \, \dfrac{dr}{dx}}{1 + \left(\dfrac{dr}{dx} \right)^2} \, \sin 2\,\alpha \qquad (B2)$$

Also, from reference 13,

$$\Delta F_t = \rho \pi r (u_x u_t + v_x v_t) \tag{B3}$$

where

u_x, v_x velocity components at the plane of symmetry of the flow due to the longitudinal motion

u_t, v_t velocity components at the plane of symmetry of the flow due to the transverse motion

Eliminating ΔF_t in equations (B2) and (B3), and using the relation

$$\frac{v_t}{u_t} = \frac{v_x}{u_x} = \frac{dr}{dx} \tag{B4}$$

the expression for u_t in incompressible flow becomes

$$\frac{u_t}{U_0} = \frac{\dfrac{dr}{dx} \sin 2\alpha}{\dfrac{u_x}{U_0} \left[1 + \left(\dfrac{dr}{dx} \right)^2 \right]^2} \tag{B5}$$

To calculate the velocity components in compressible flow by linear theory, the procedure used in Appendix A can be extended to the inclined body with only one important difference. In linear theory one coordinate axis must be in the free–stream direction (reference 7), since all coordinates normal to this axis are reduced by the factor β. When a body of revolution is inclined to the stream direction and its coordinates normal to the stream direction are reduced by the factor β, it does not remain a body of revolution. For slender bodies at small angles of attack, however, this distortion from a body of revolution is small and was ignored in this calculation. The incompressible flow was considered about a body of revolution, the radial ordinates of which were β times the radial ordinates of the body in compressible flow, and the angle of attack α' of which was related to the angle of attack in compressible flow α by

$$\tan \alpha' = \beta \tan \alpha \tag{B6}$$

where

β $\sqrt{1-M_0^2}$

M_0 free–stream Mach number

Applying equation (B5) to this body gives

$$\frac{u_t{}'}{U_o} = \frac{\dfrac{dr'}{dx} \sin 2\alpha'}{\dfrac{u_x{}'}{U_o}\left[1 + \left(\dfrac{dr'}{dx}\right)^2\right]^2} \tag{B7}$$

where the primes indicate that all radial ordinates and the angle of attack of the original body have been reduced by the factor β. It is apparent that

$$\frac{dr'}{dx} = \frac{d(\beta r)}{dx} = \beta\,\frac{dr}{dx}$$

and it is consistent with linear theory to consider

$$\sin 2\alpha' \cong 2\beta\alpha$$

$$\left(\frac{dr}{dx}\right)^2 \cong 0$$

$$\frac{u_x{}'}{U_o} = 1 + \left(\frac{\Delta u_x}{U_o}\right)' = 1 + \beta^2\left(\frac{\Delta u_x}{U_o}\right)$$

and

$$\frac{\Delta u_x}{U_o} \cong \left(\frac{\Delta u}{U_o}\right)_{\alpha=0}$$

where $\left(\dfrac{\Delta u}{U_o}\right)_{\alpha=0}$ is obtained from equations (A15) and (A16) at the same Mach number under consideration.

Inserting these approximations into equation (B7) results in

$$\frac{u_t{}'}{U_o} = \frac{\beta^2\,2\alpha\,\dfrac{dr}{dx}}{1 + \beta^2\left(\dfrac{\Delta u}{U_o}\right)_{\alpha=0}} \tag{B8}$$

and from equations (A10) and (A11)

$$\frac{u_t}{U_0} = \frac{1}{\beta^2} \frac{u_t{}'}{U_0} = \frac{2\alpha \frac{dr}{dx}}{1 + \beta^2 \left(\frac{\Delta u}{U_0}\right)_{\alpha=0}} \tag{B9}$$

which indicates that the induced velocities due to angle of attack are practically unaffected by compressibility.

The pressure coefficients along the upper meridian in compressible flow calculated by linear theory then become

$$P = -2 \left[\left(\frac{\Delta u}{U_0}\right)_{\alpha=0} + \frac{u_t}{U_0} \right] \tag{B10}$$

and along the lower meridian

$$P = -2 \left[\left(\frac{\Delta u}{U_0}\right)_{\alpha=0} - \frac{u_t}{U_0} \right] \tag{B11}$$

The result of these calculations is shown graphically in figure 11.

REFERENCES

1. Hieser, Gerald, and Whitcomb, Charles F.: Investigation of the Effects of a Nacelle on the Aerodynamic Characteristics of a Swept Wing and the Effects of Sweep on the Wing Alone. NACA TN 1709, 1948.

2. Dannenberg, Robert E., and Blackaby, James R.: An Experimental Investigation of a Jet-Engine Nacelle in Several Positions on a 37.25° Swept-Back Wing. NACA RM A50A13, 1950.

3. Edwards, George G., and Boltz, Frederick W.: An Analysis of the Forces and Pressure Distribution on a Wing With the Leading Edge Swept Back 37.25°. NACA RM A9K01, 1949.

4. Sivells, James C., and Deters, Owen J.: Jet-Boundary and Plan-Form Corrections for Partial-Span Models with Reflection Plane, End Plate, or No End Plate in a Closed Circular Wind Tunnel. NACA Rep. 843, 1946.

5. Herriot, John G.: Blockage Corrections for Three-Dimensional-Flow Closed-Throat Wind Tunnels, with Consideration of the Effect of Compressibility. NACA RM A7B28, 1947.

6. Beals, Donald B., and Mourhess, Mary J: Numerical Evaluation of the Wake-Survey Equations for Subsonic Flow Including the Effect of Energy Addition. NACA ARR L5H27, 1945.

7. Hess, Robert V., and Gardner, Clifford S: Study by the Prandtl-Glauert Method of Compressibility Effects and Critical Mach Number for Ellipsoids of Various Aspect Ratios and Thickness Ratios. NACA TN 1792, 1949.

8. Allen, H. Julian: Pressure Distribution and Some Effects of Viscosity on Slender Inclined Bodies of Revolution. NACA TN 2044, 1950.

9. Munk, Max M.: Fluid Mechanics, Part II, Ellipsoids of Revolution. Vol. I of Aerodynamic Theory, div. C, ch. VII, sec. 6; W. F. Durand ed., Julius Springer, (Berlin) 1935, pp. 284-285.

10. Abbott, Ira H.: Fuselage-Drag Tests in the Variable-Density Wind Tunnel. NACA TN 614, 1937.

11. Prandtl, L: Applications of Modern Hydrodynamics to Aeronautics. NACA Rep. 116, 1921.

12. Upson, Ralph H., and Klikoff, W. A.: Application of Practical Hydrodynamics to Airship Design. NACA Rep. 405, 1931.

13. von Kármán, Theodore: Calculation of Pressure Distribution on Airship Hulls. NACA TM 574, 1930.

TABLE I

COORDINATES FOR THE NACA 64_1-212 AIRFOIL
[Stations and ordinates given in
percent of airfoil chord]

Upper surface		Lower surface	
Station	Ordinate	Station	Ordinate
0	0	0	0
.418	1.025	.582	-.925
.659	1.245	.841	-1.105
1.147	1.593	1.353	-1.379
2.382	2.218	2.618	-1.846
4.868	3.123	5.132	-2.491
7.364	3.815	7.636	-2.967
9.865	4.386	10.135	-3.352
14.872	5.291	15.128	-3.945
19.886	5.968	20.114	-4.376
24.903	6.470	25.097	-4.680
29.921	6.815	30.079	-4.871
34.941	7.008	35.059	-4.948
39.961	7.052	40.039	-4.910
44.982	6.893	45.018	-4.703
50.000	6.583	50.000	-4.377
55.016	6.151	54.984	-3.961
60.029	5.619	59.971	-3.477
65.039	5.004	64.961	-2.944
70.045	4.322	69.955	-2.378
75.047	3.590	74.953	-1.800
80.045	2.825	79.955	-1.233
85.038	2.054	84.962	-.708
90.027	1.303	89.973	-.269
95.013	.604	94.987	.028
100.000	0	100.000	0

L.E. radius: 1.040. Slope of radius
through L.E.: 0.084.

TABLE II

COORDINATES FOR THE NACELLE AND THE BODY OF REVOLUTION
[Stations and ordinates given in
percent of body length]

Station	Nacelle ordinate	Body of revolution ordinate
0	0	0
1.25	1.62	1.62
2.50	2.29	2.29
5.00	3.16	3.16
10.00	4.31	4.31
20.00	5.62	5.62
30.00	6.26	6.26
38.00	7.69	7.69
40.00	7.69	7.69
50.00	7.63	7.46
60.00	7.15	6.83
70.00	6.08	5.65
80.00	4.36	3.96
85.00	3.32	3.02
90.00	2.27	2.04
95.00	1.14	1.03
97.50	.54	.52
100.00	0	0

1.50 Dia

6.00

35.30

39.00

Coordinates in table II

(a) Body of revolution.

Semispan area (wing alone) = 8.283 sq ft
Aspect ratio (wing alone) = 6.04
Taper ratio = 0.50
c̄(wing alone) = 1.728 ft
        (parallel to root chord)

13.33

5.33

25 percent chord
   of airfoil section

NACA 64₁-212
   airfoil section

90°

39.00

9.00

60.00

55.00

44.00

33.00

18.60

0.25c̄

9.00

6.00

37.25°

35.00°

28.85°

10.66

25.48

26.67

Rows of pressure orifices

All dimensions are in inches
   unless otherwise noted

Coordinates in tables I and II

(b) Semispan wing and nacelle.

NACA

Figure 1.—Body of revolution and wing-nacelle combination.
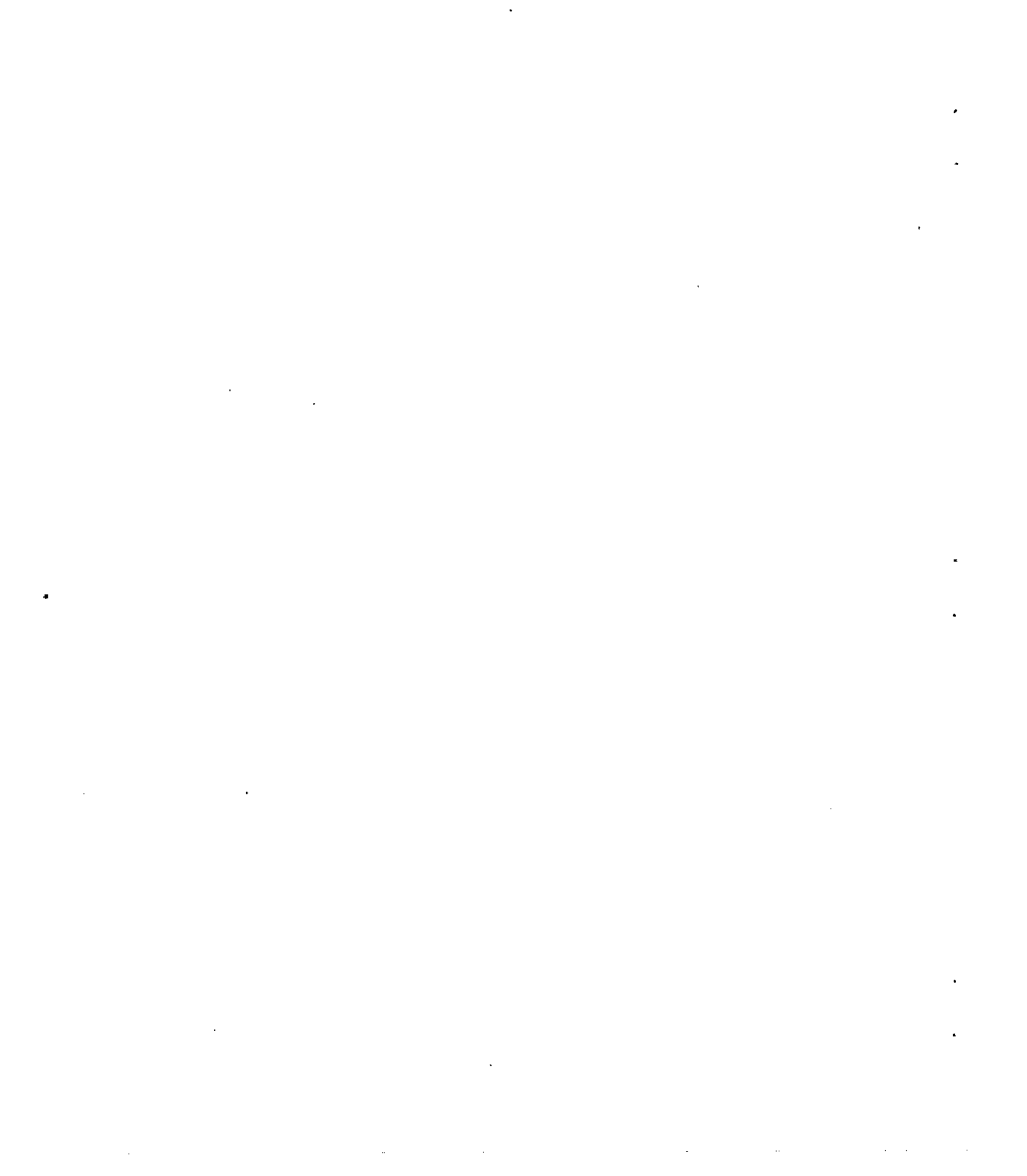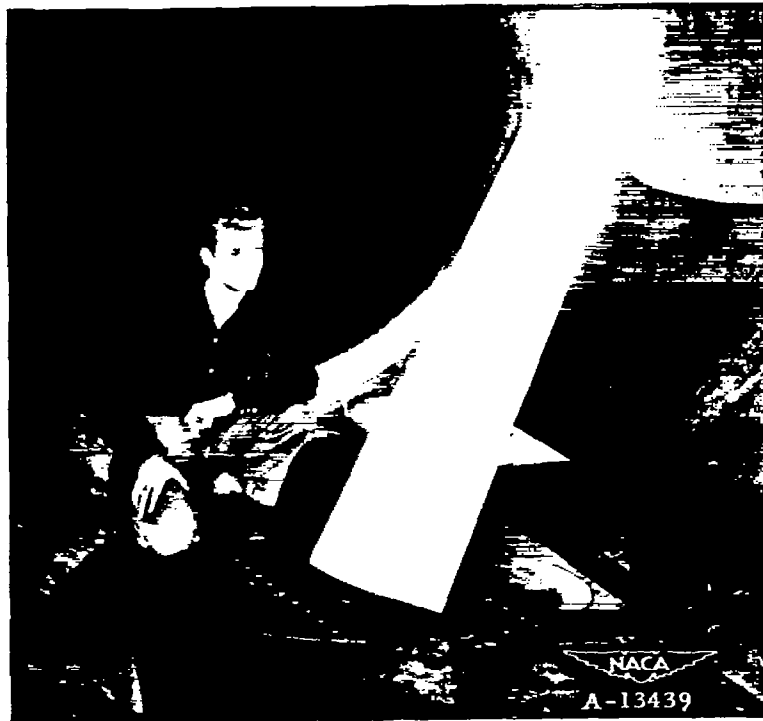
(a) Wing-nacelle combination.

(b) Body of revolution.

Figure 2.— Wing-nacelle combination and body of revolution mounted in the
       Ames 12-foot pressure wind tunnel.
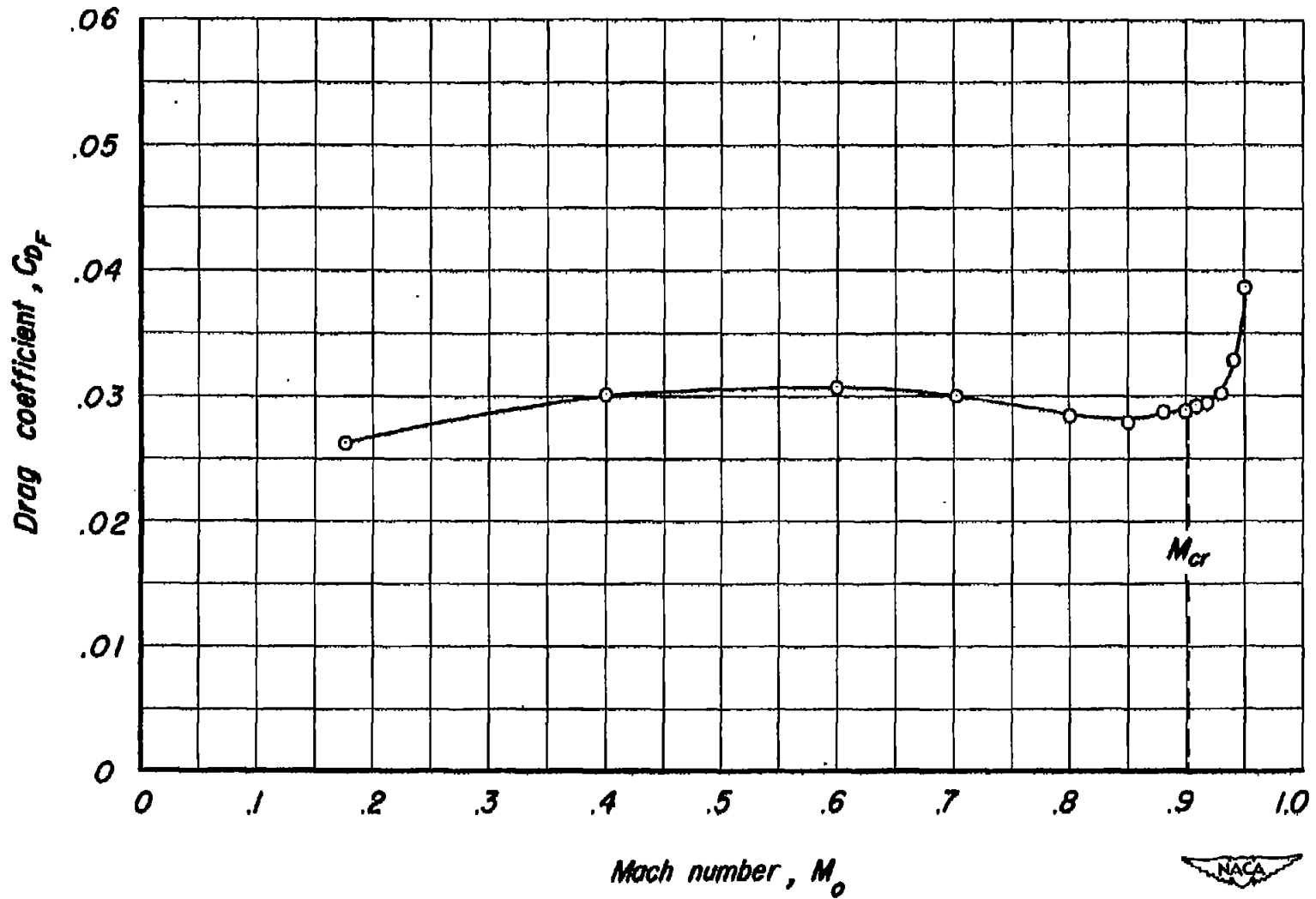
Figure 3.—The variation of drag coefficient with Mach number for the body of revolution at 0° angle of attack. R_b, 3,760,000.
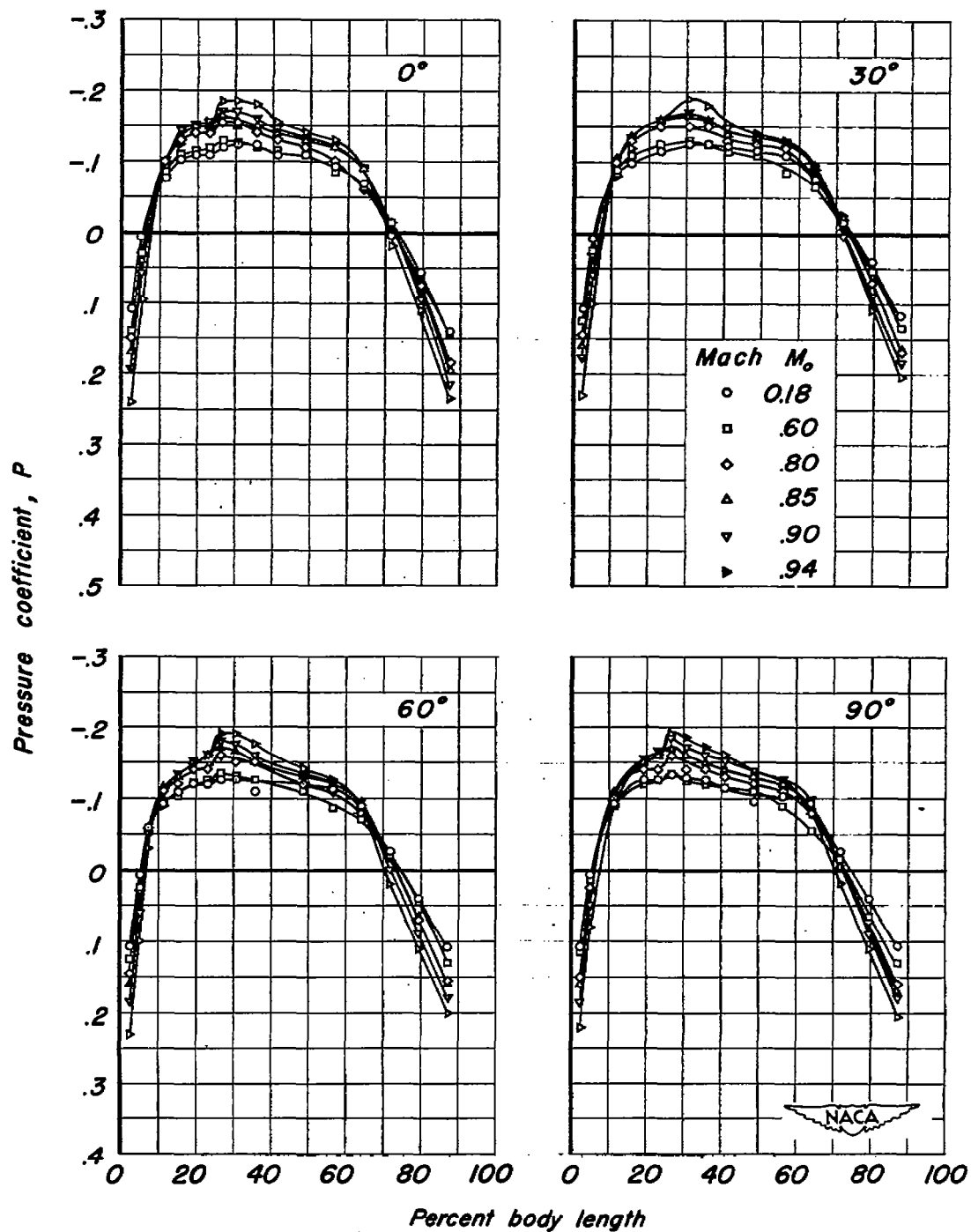
Figure 4.- The distribution of pressure coefficient along four meridians on the
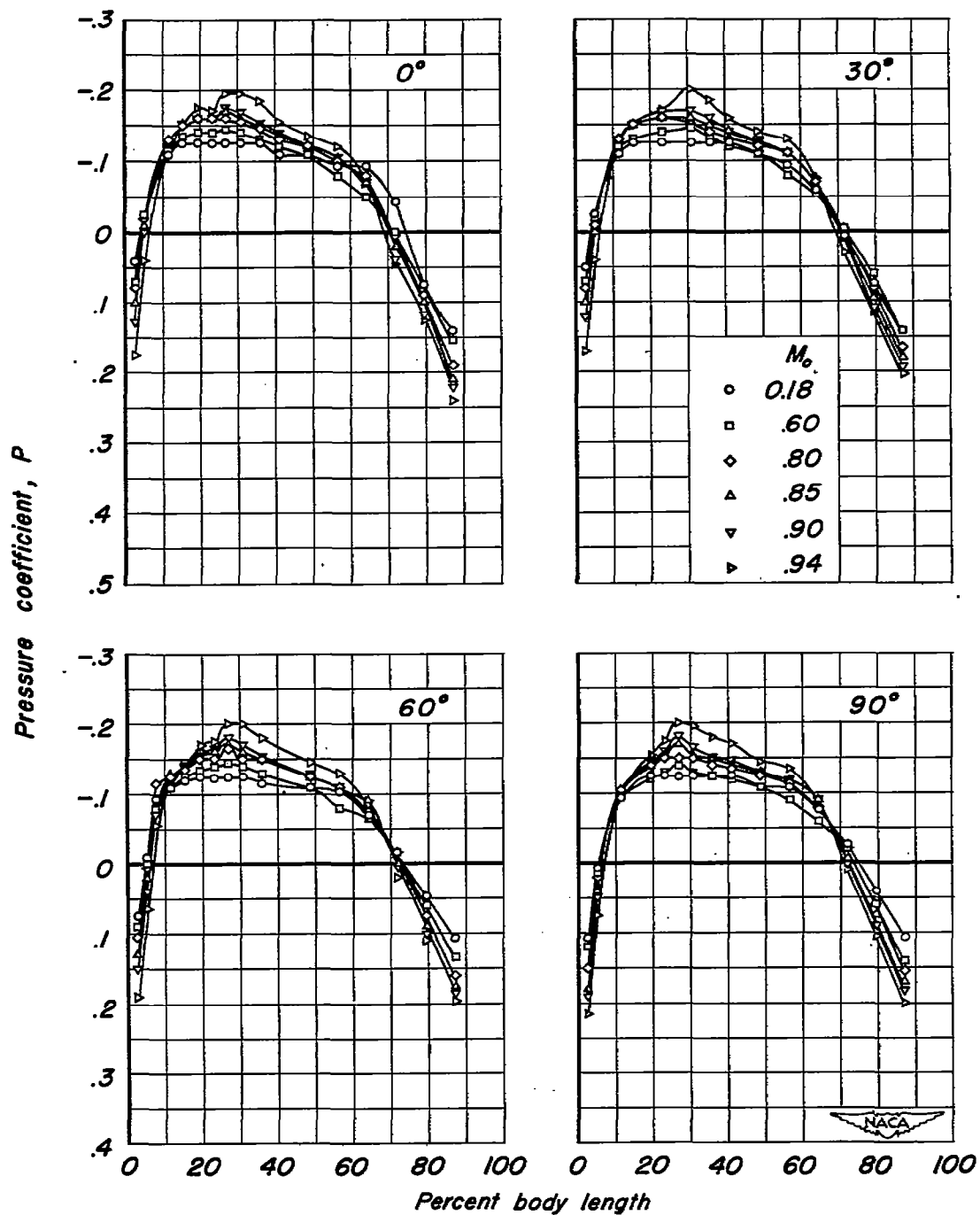
(a) Meridians, 0°, 30°, 60°, 90°.

Figure 5.- The distribution of pressure coefficient along eight meridians on the body of revolution at several Mach numbers. α_u, 2°.
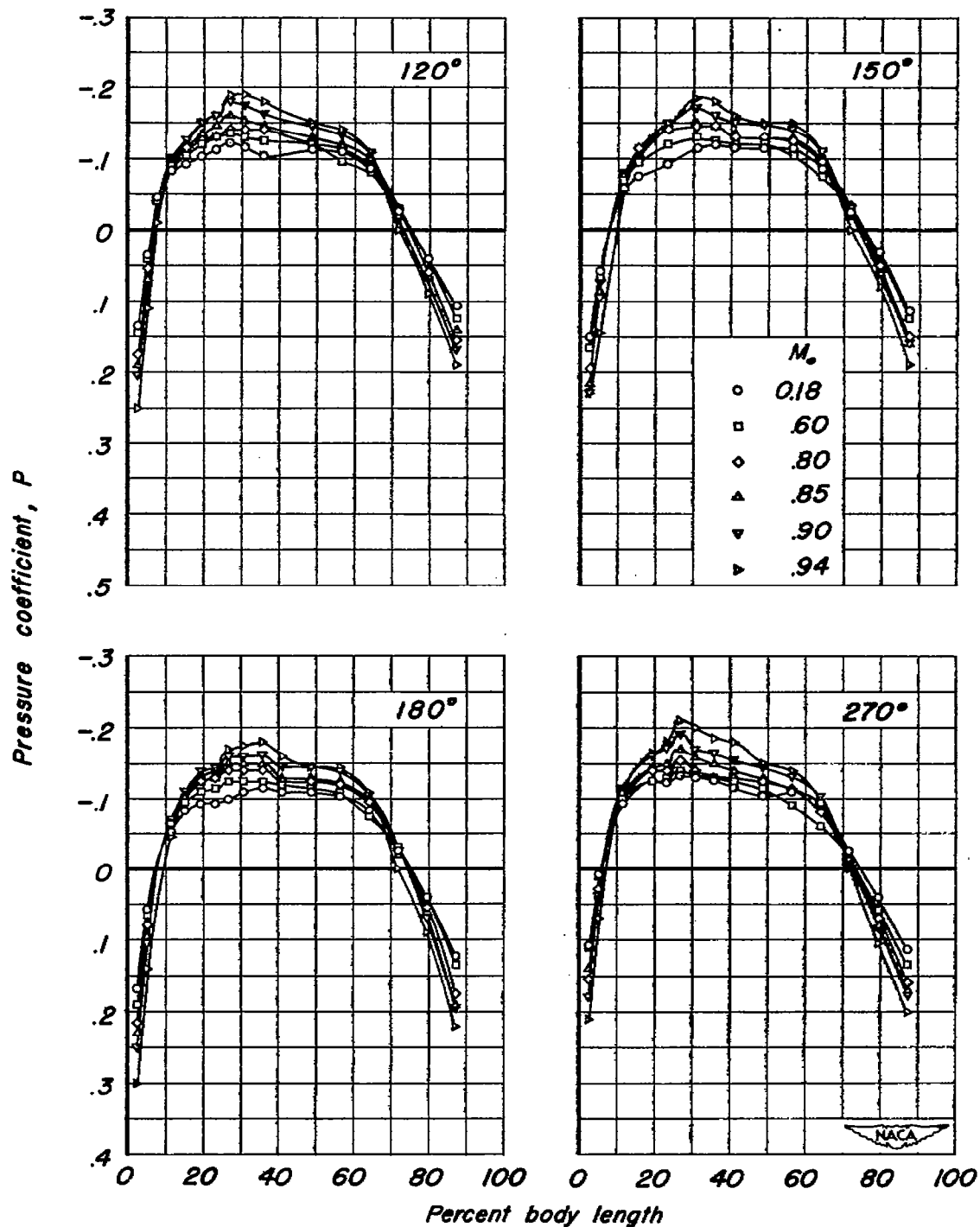
(b) Meridians, 120°, 150°, 180°, 270°

Figure 5.- Concluded.
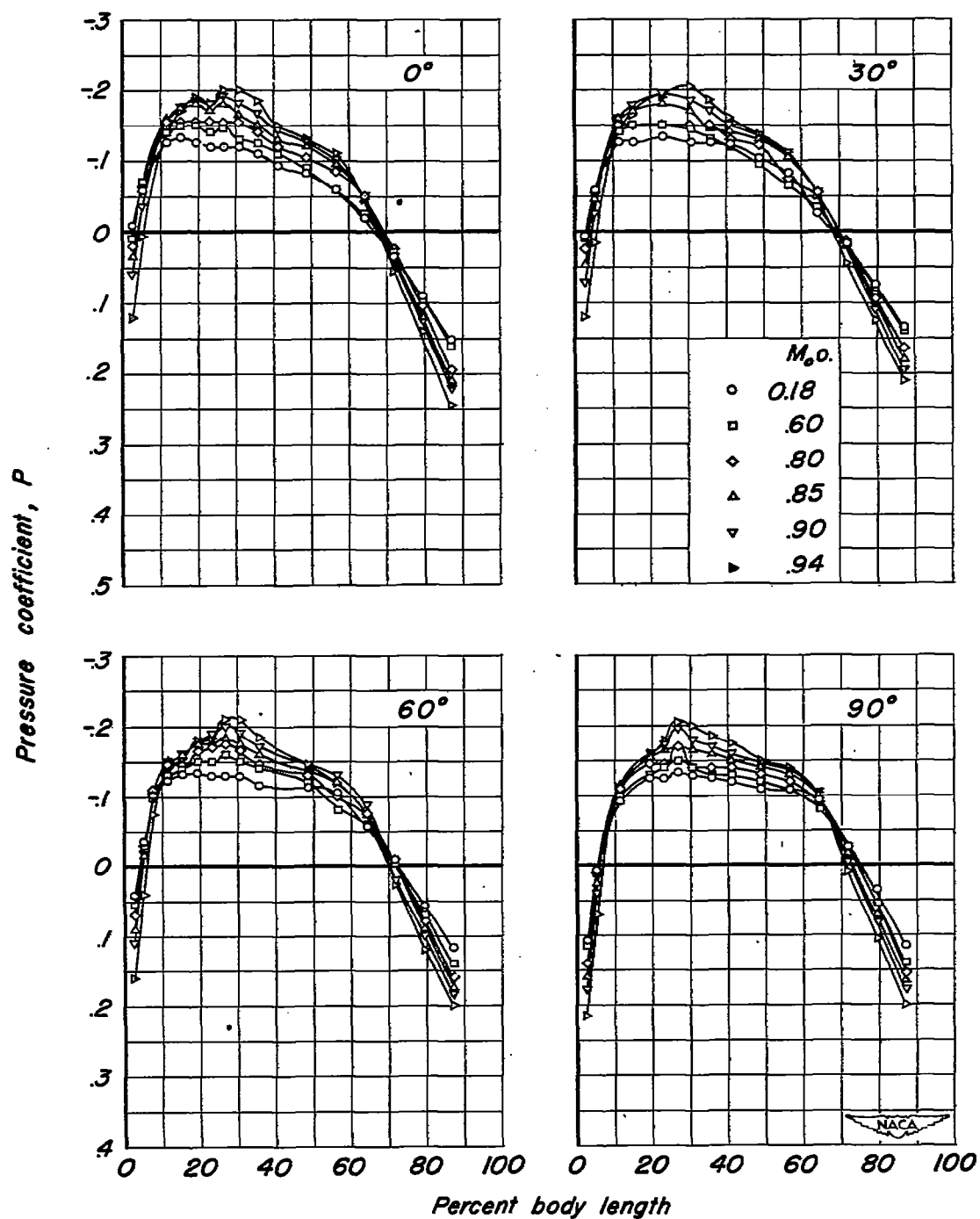
(a) Meridians, 0°, 30°, 60°, 90°.

Figure 6.— The distribution of pressure coefficient along eight meridians on the body of revolution at several Mach numbers. a_u, 4°.
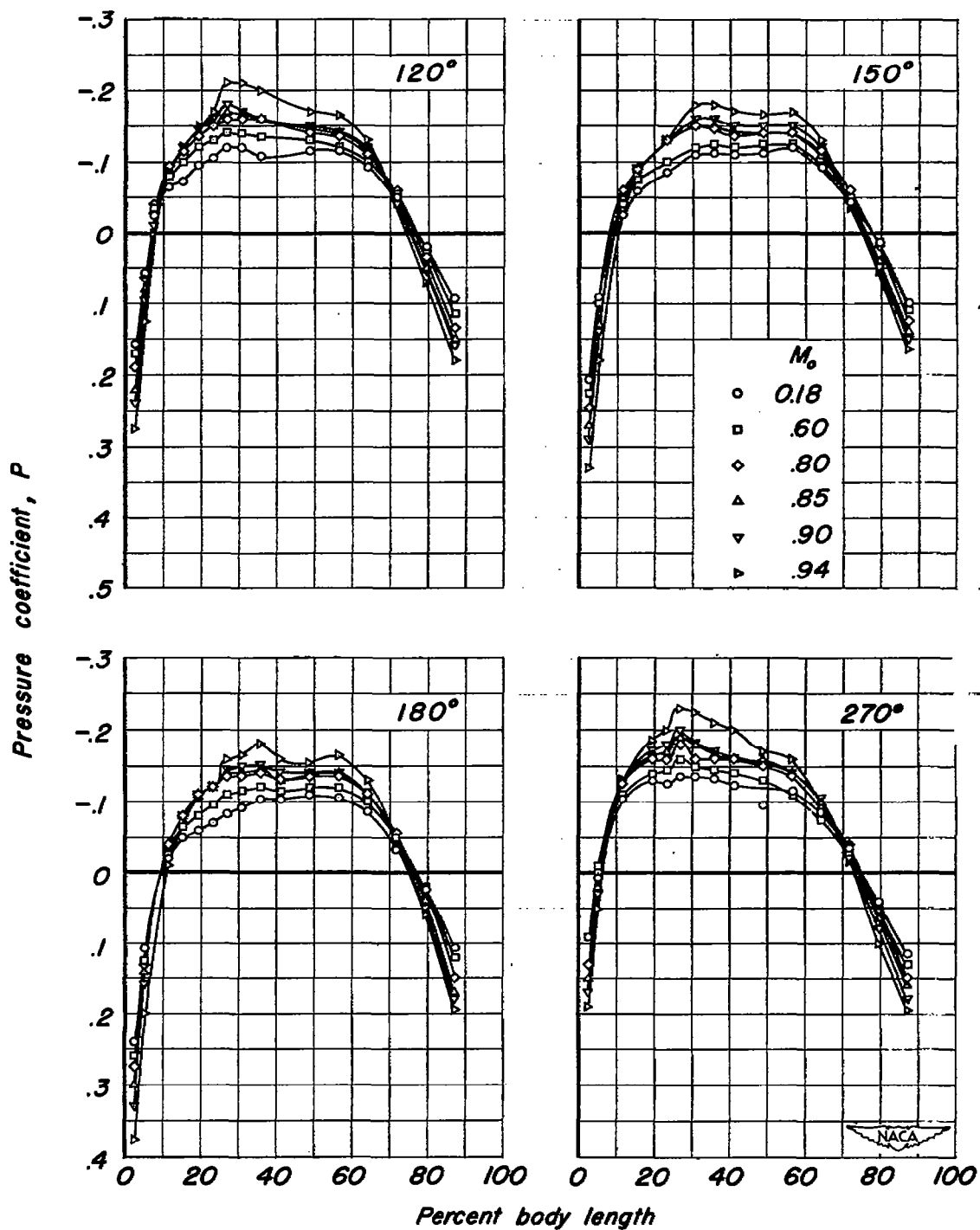
(b) Meridians, 120°, 150°, 180°, 270°.

Figure 6.- Concluded.
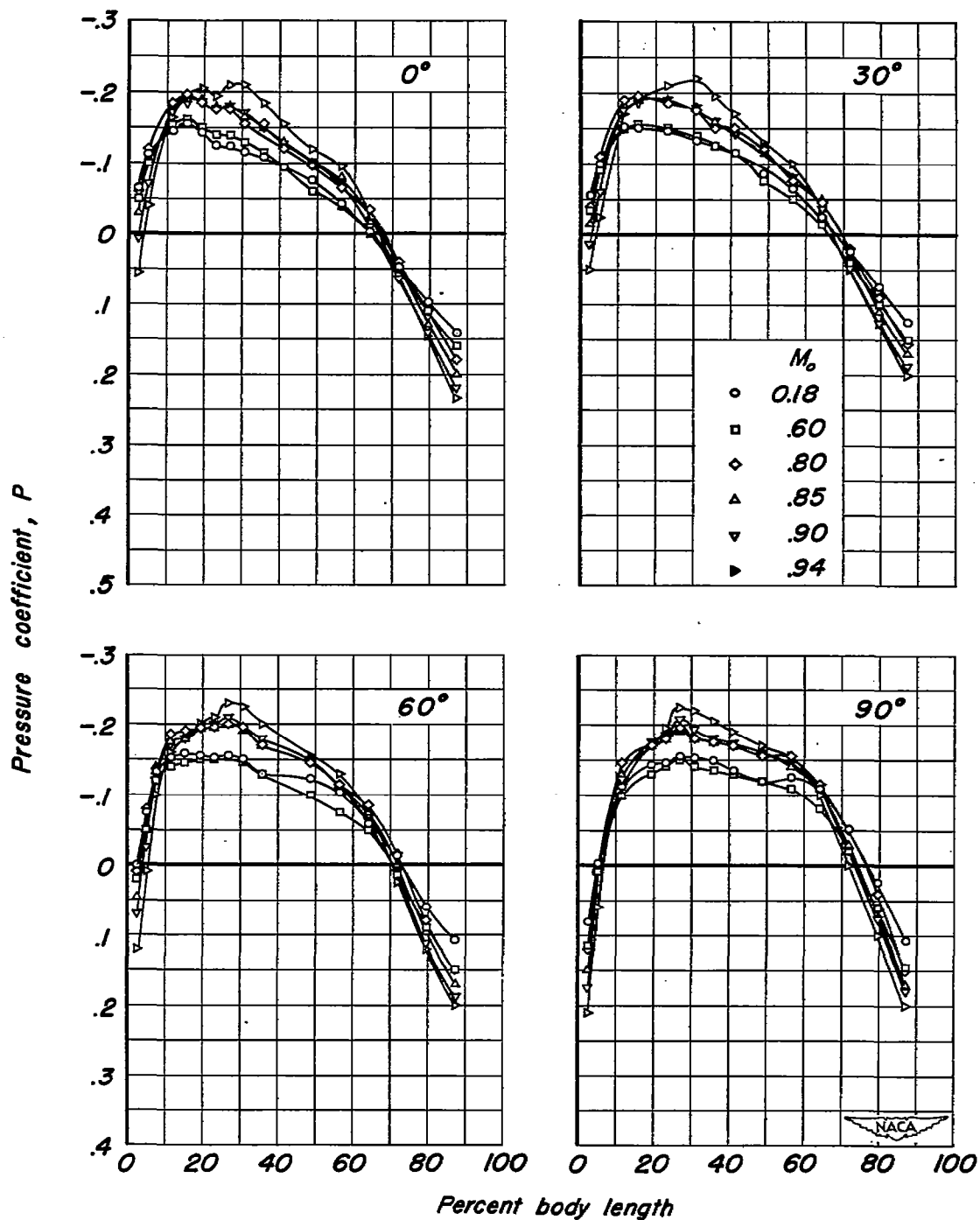
(a) Meridians, 0°, 30°, 60°, 90°.

Figure 7.- The distribution of pressure coefficient along eight meridians on the body of revolution at several Mach numbers. a_u, 6°.
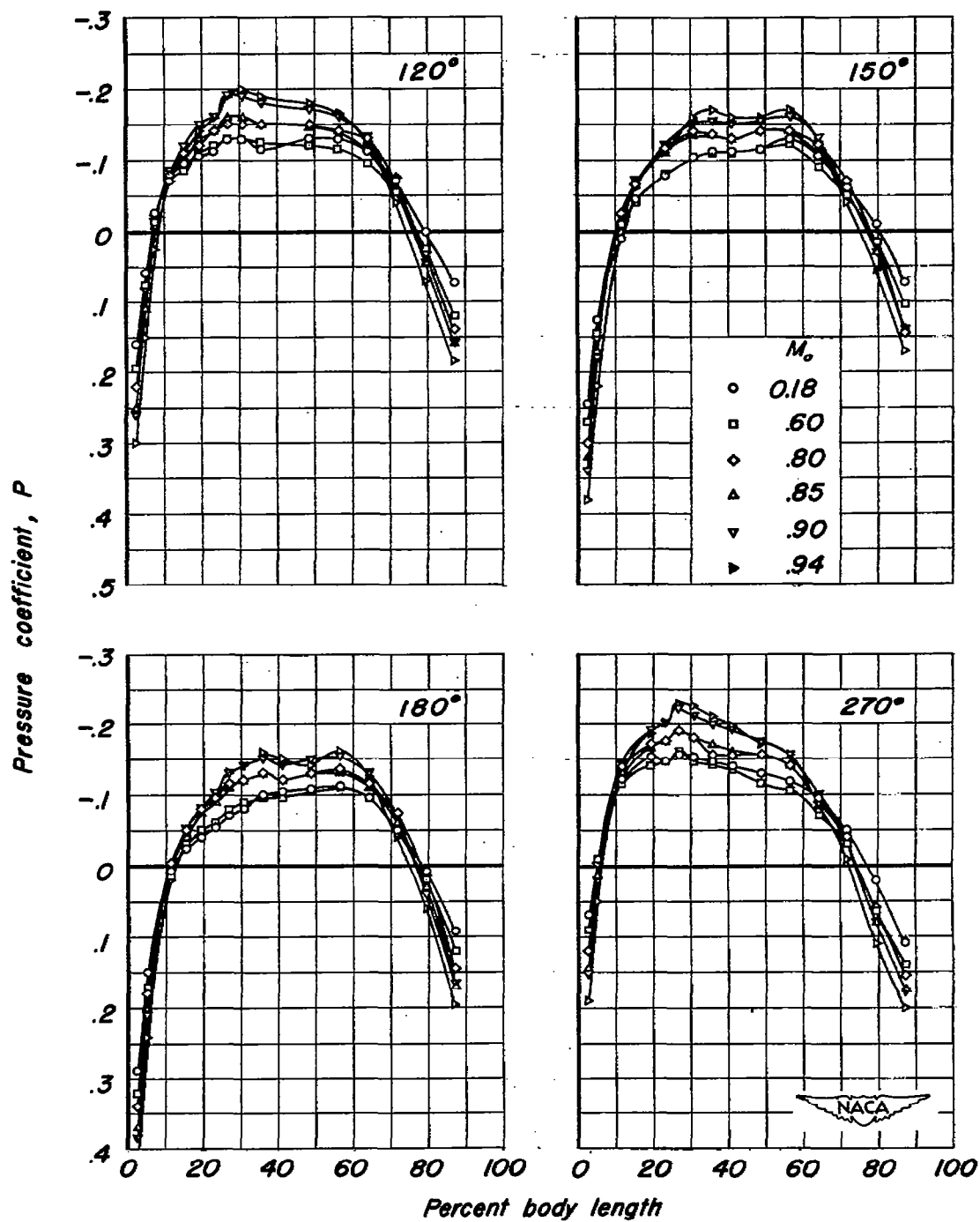
(b) Meridians, 120°, 150°, 180°, 270°

Figure 7. - Concluded.
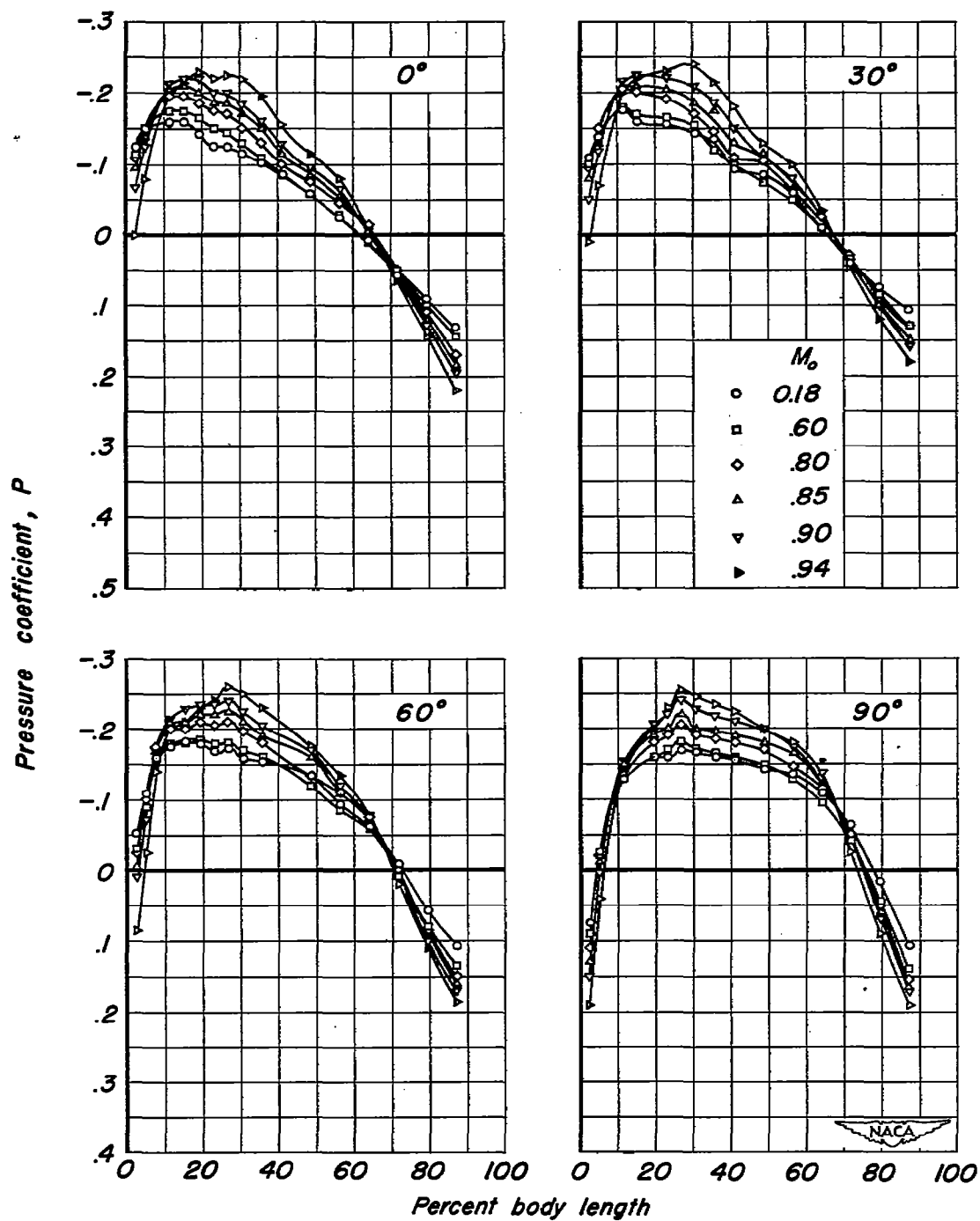
(a) Meridians, 0°, 30°, 60°, 90°.

Figure 8.- The distribution of pressure coefficient along eight meridians on the body of revolution at several Mach numbers. a_u, 8°.
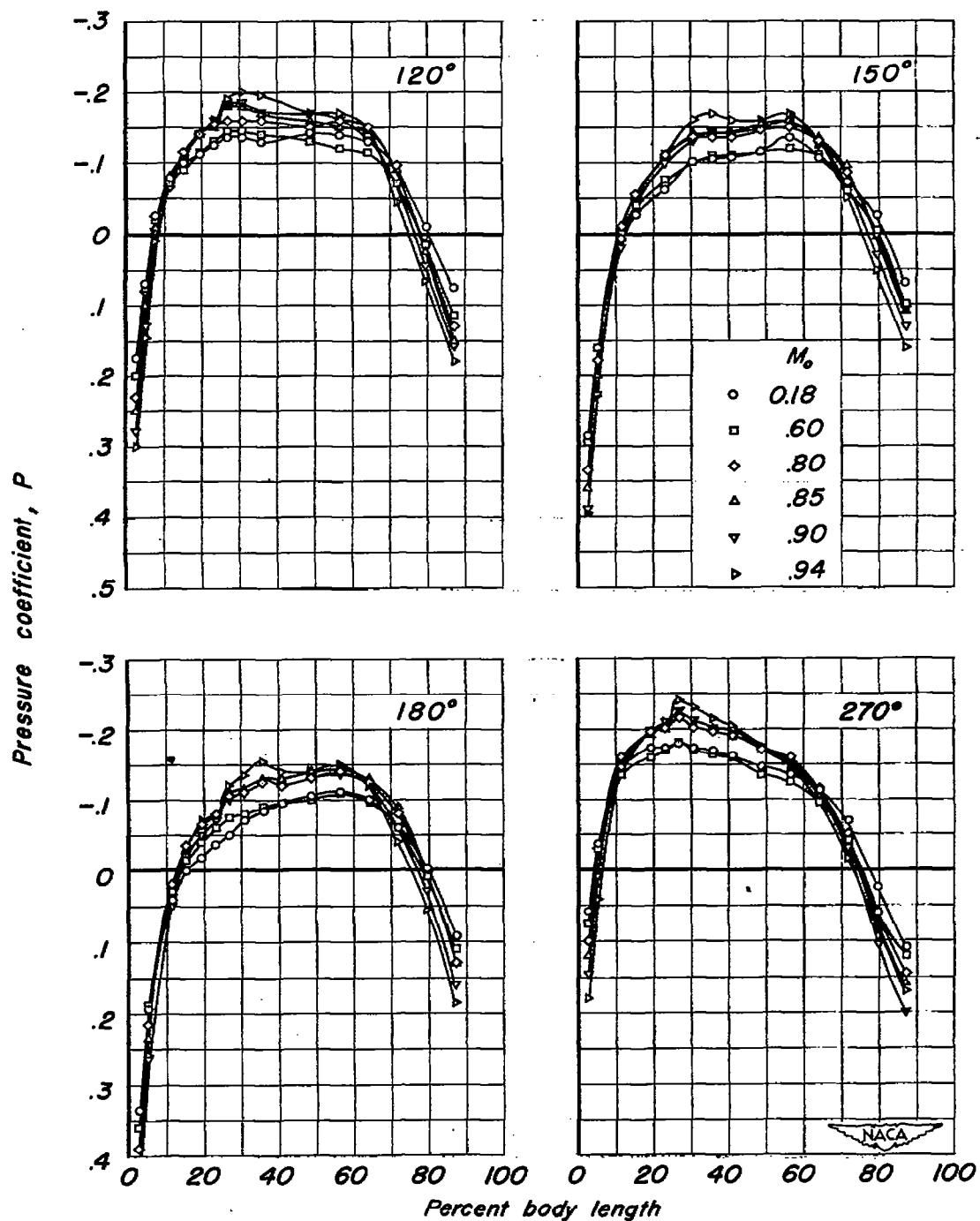
(b) Meridians, 120°, 150°, 180°, 270°

Figure 8.- Concluded.
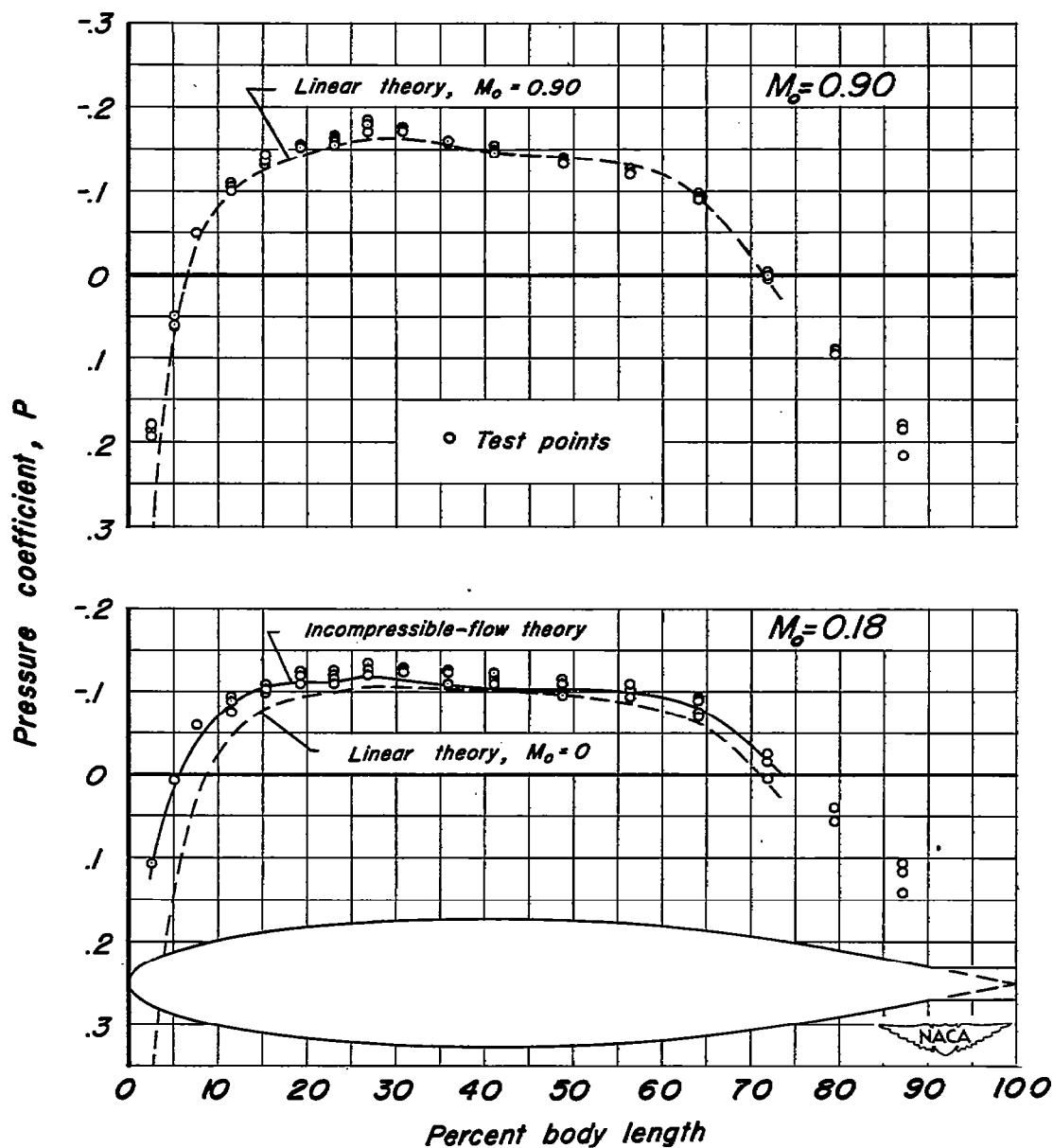
Figure 9.—A comparison of the lengthwise distribution of pressure coefficient obtained experimentally at Mach numbers of 0.18 and 0.90 with that calculated by theory. a_u, $0°$.
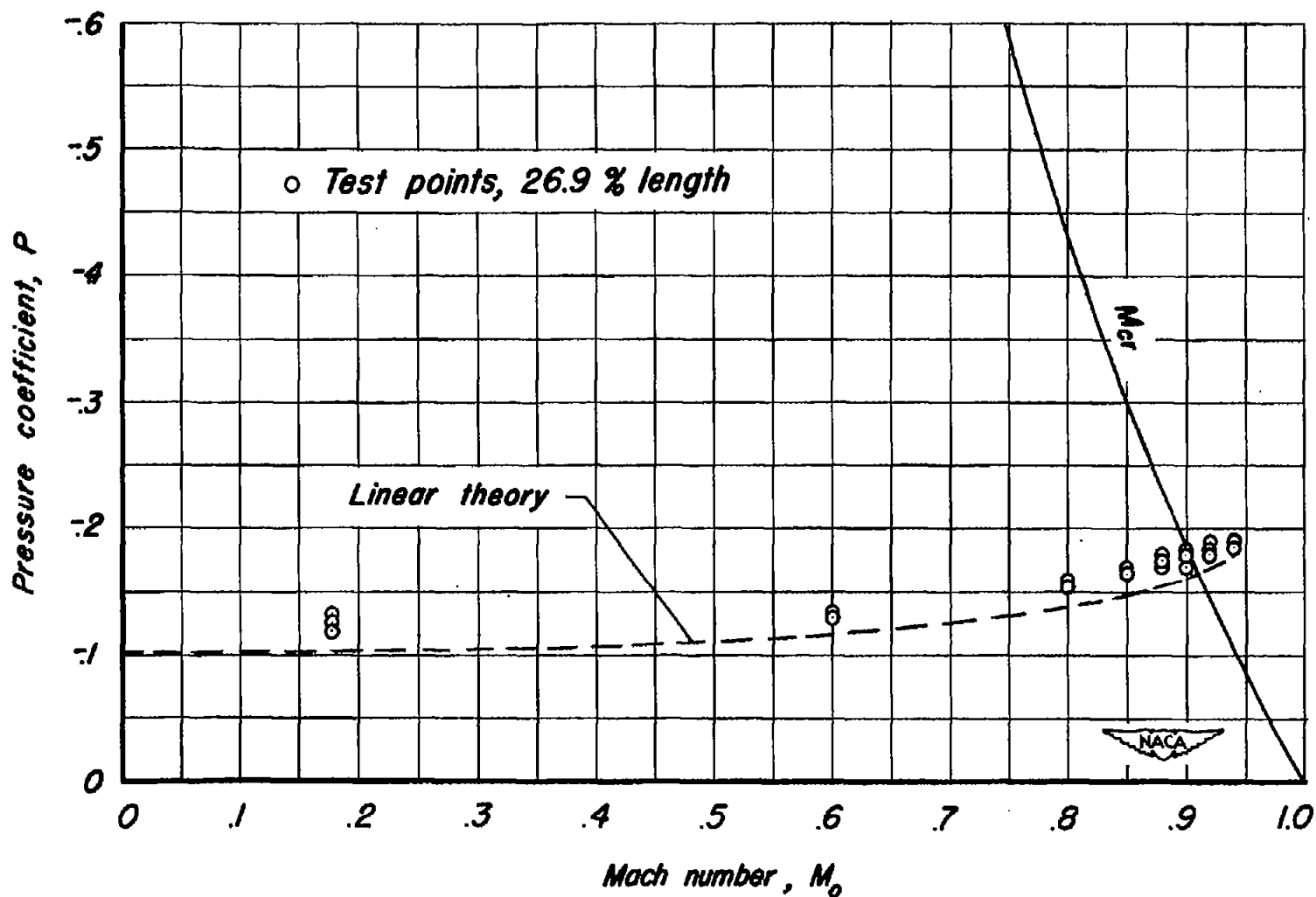
Figure 10.—The effect of Mach number on the pressure coefficients at the minimum-pressure station on the body of revolution. α_u, $0°$.
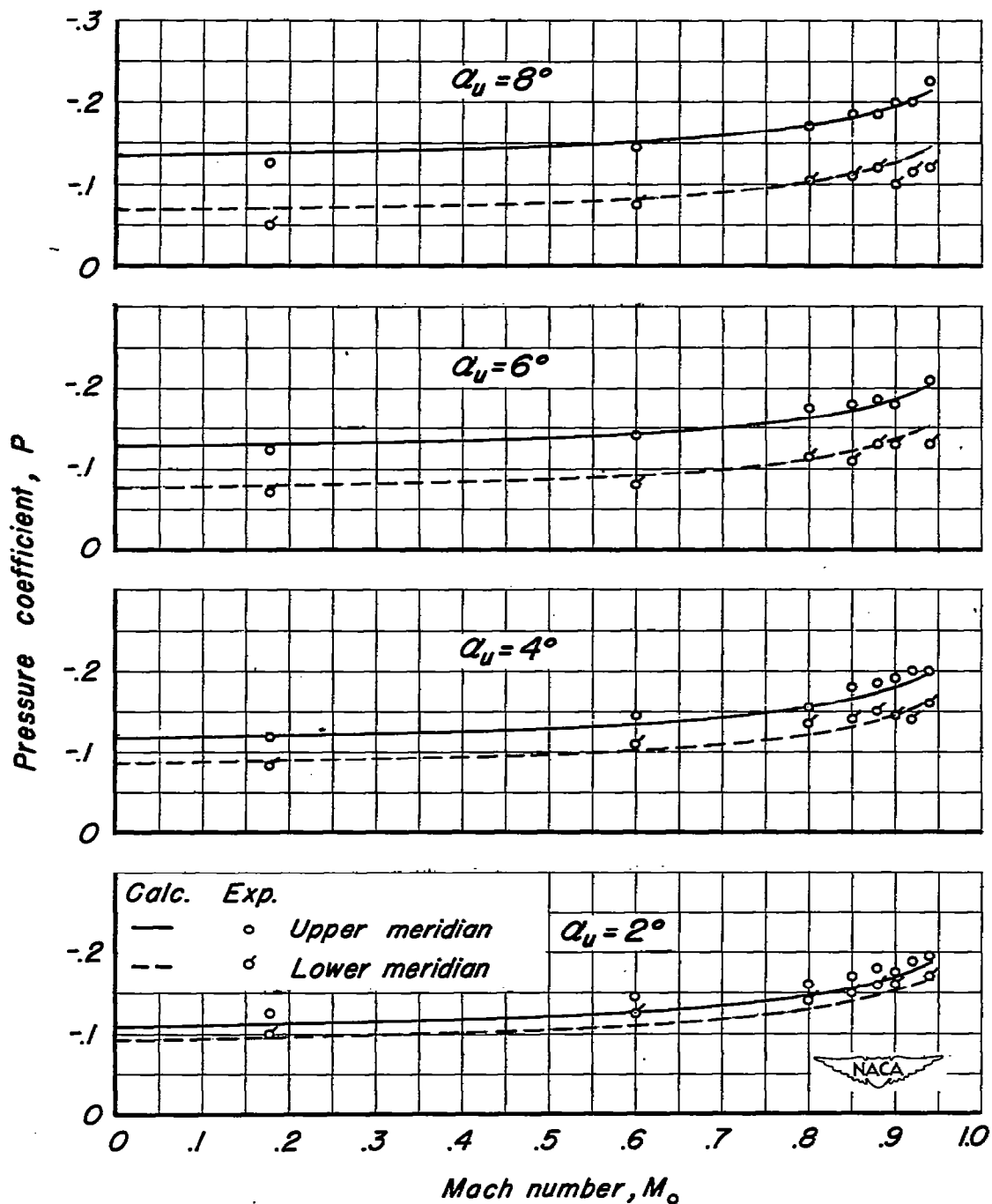
Figure II.— A comparison of the effect of Mach number on the pressure coefficient on the upper and lower surfaces at 26.9-percent length at several angles of attack with that calculated by linear theory.

(a) C_L vs a.
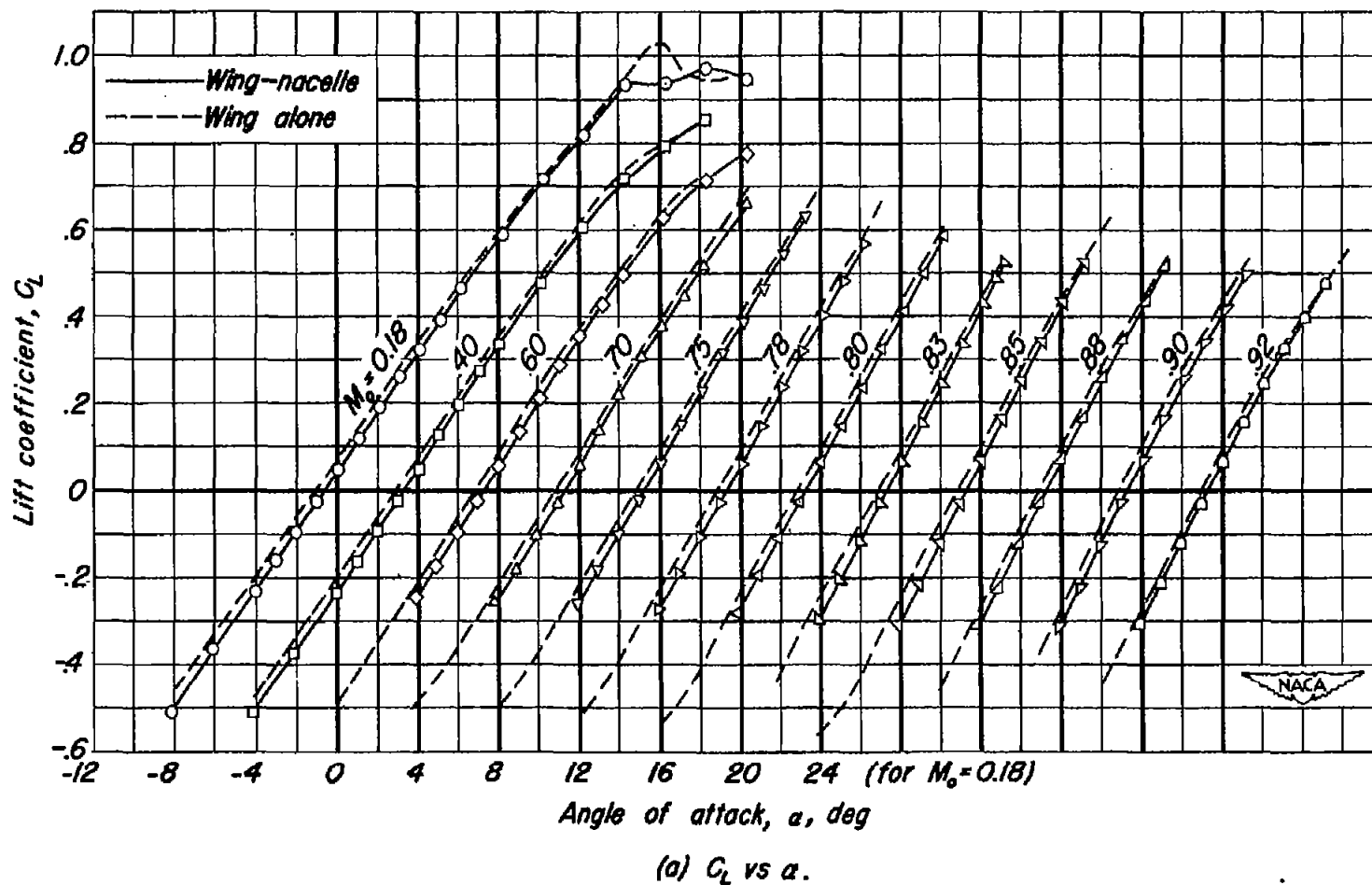
Figure 12.—The effects of Mach number on the aerodynamic characteristics of the wing-nacelle combination. R_w, 2,000,000.
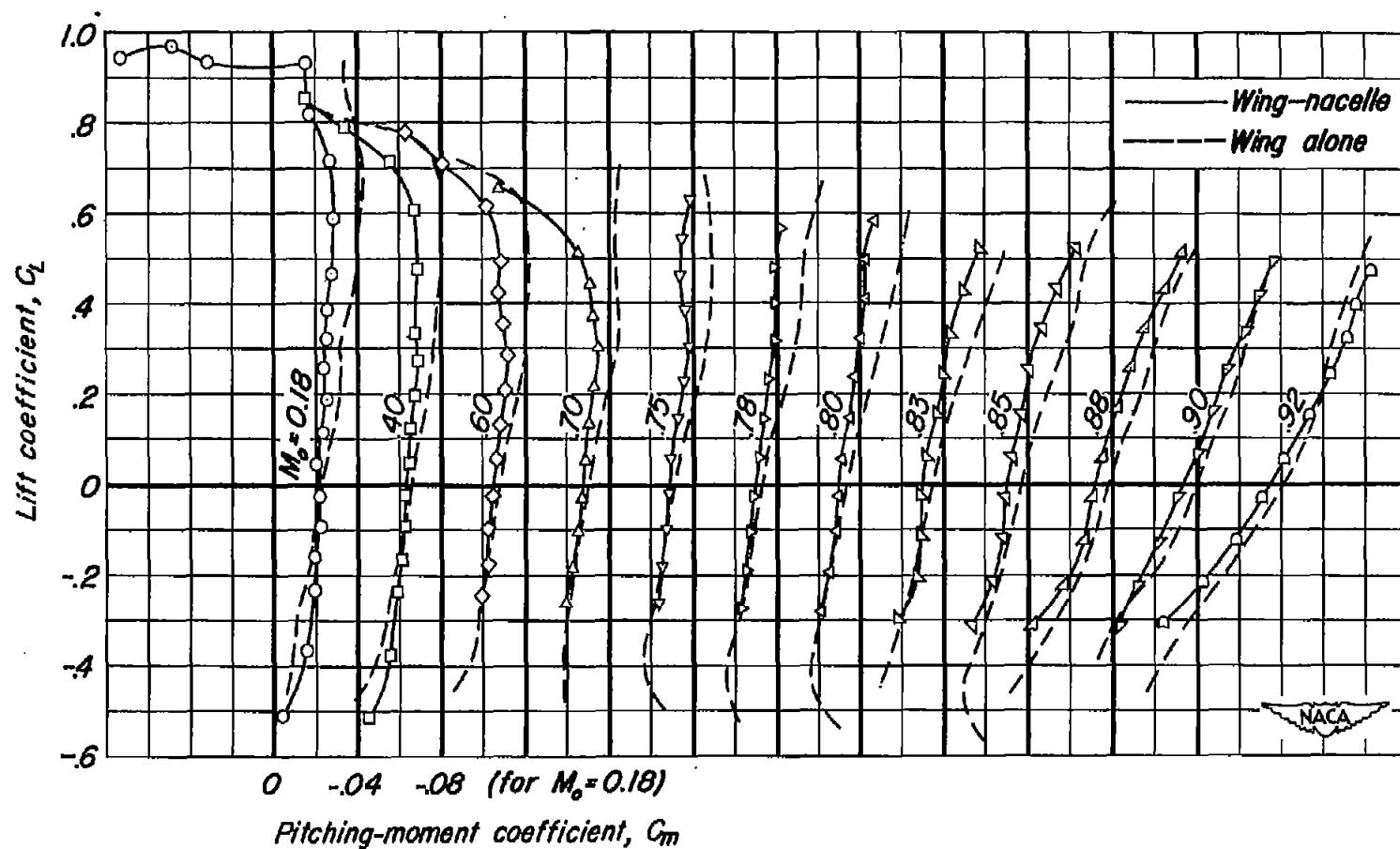
(b) C_L vs C_m.

Figure 12.—Continued.
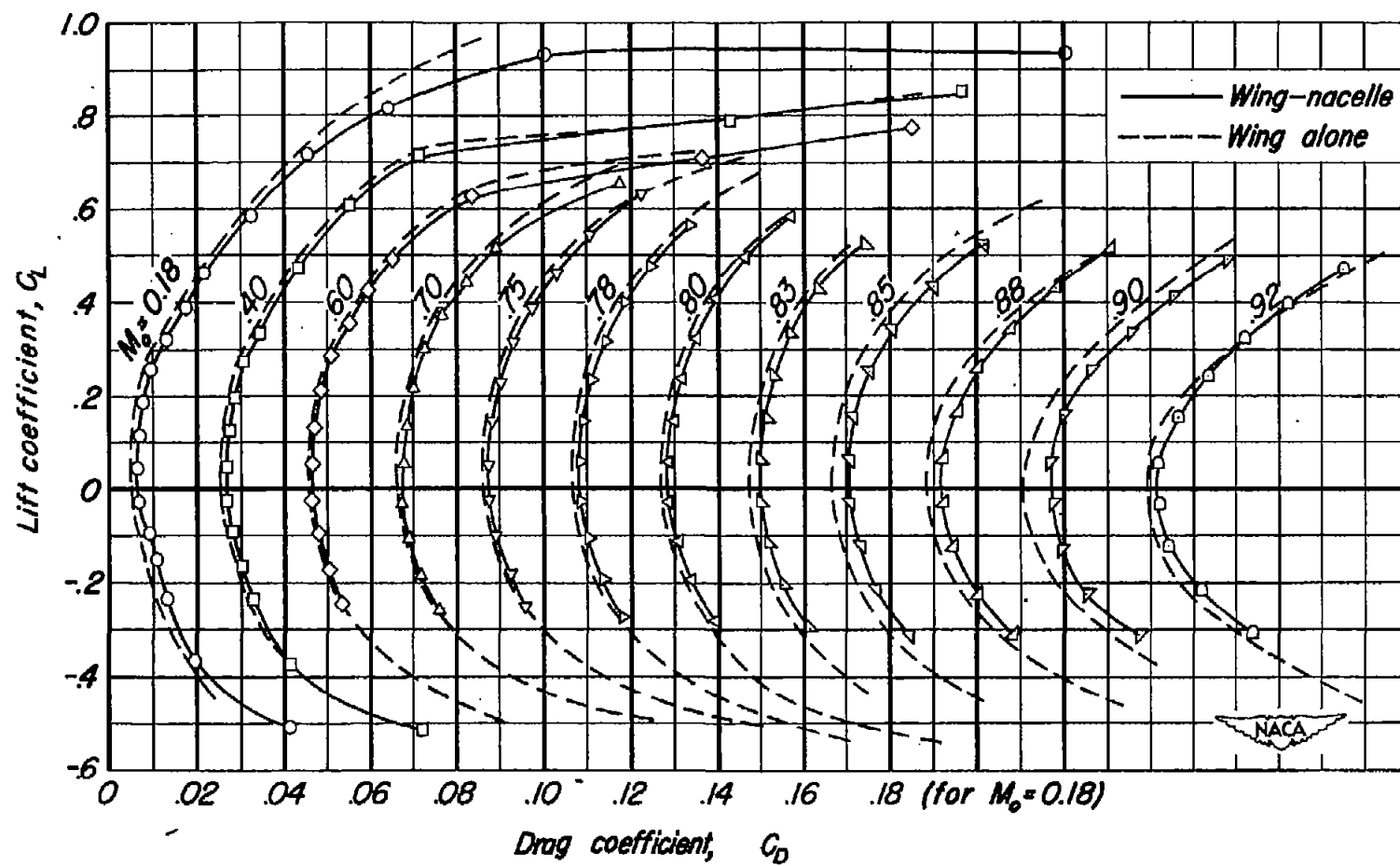
(c) C_L vs C_D.

Figure 12.- Concluded.
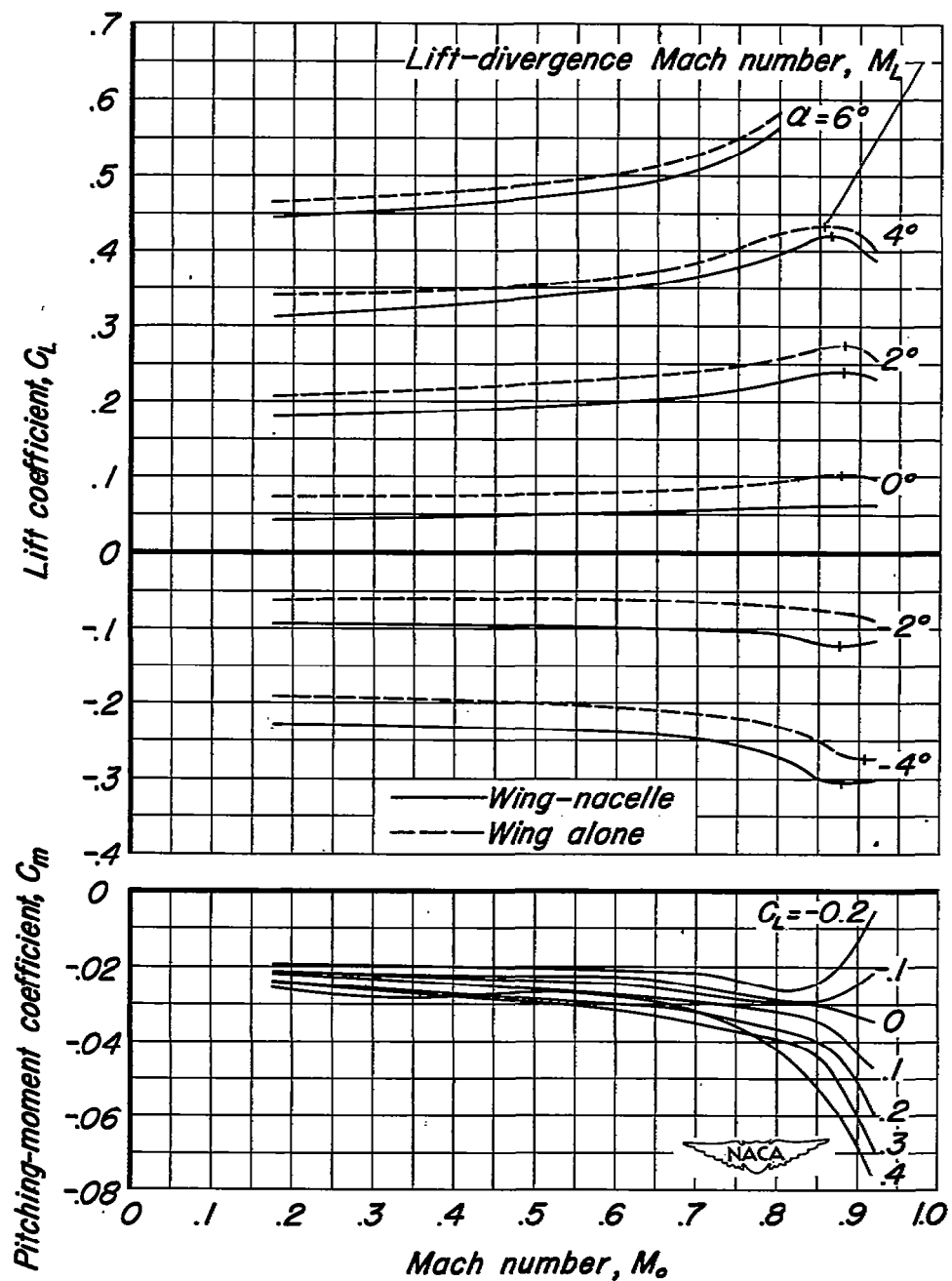
Figure 13.- The variation with Mach number of the lift coefficient at several angles of attack and of the pitching-moment coefficient at several values
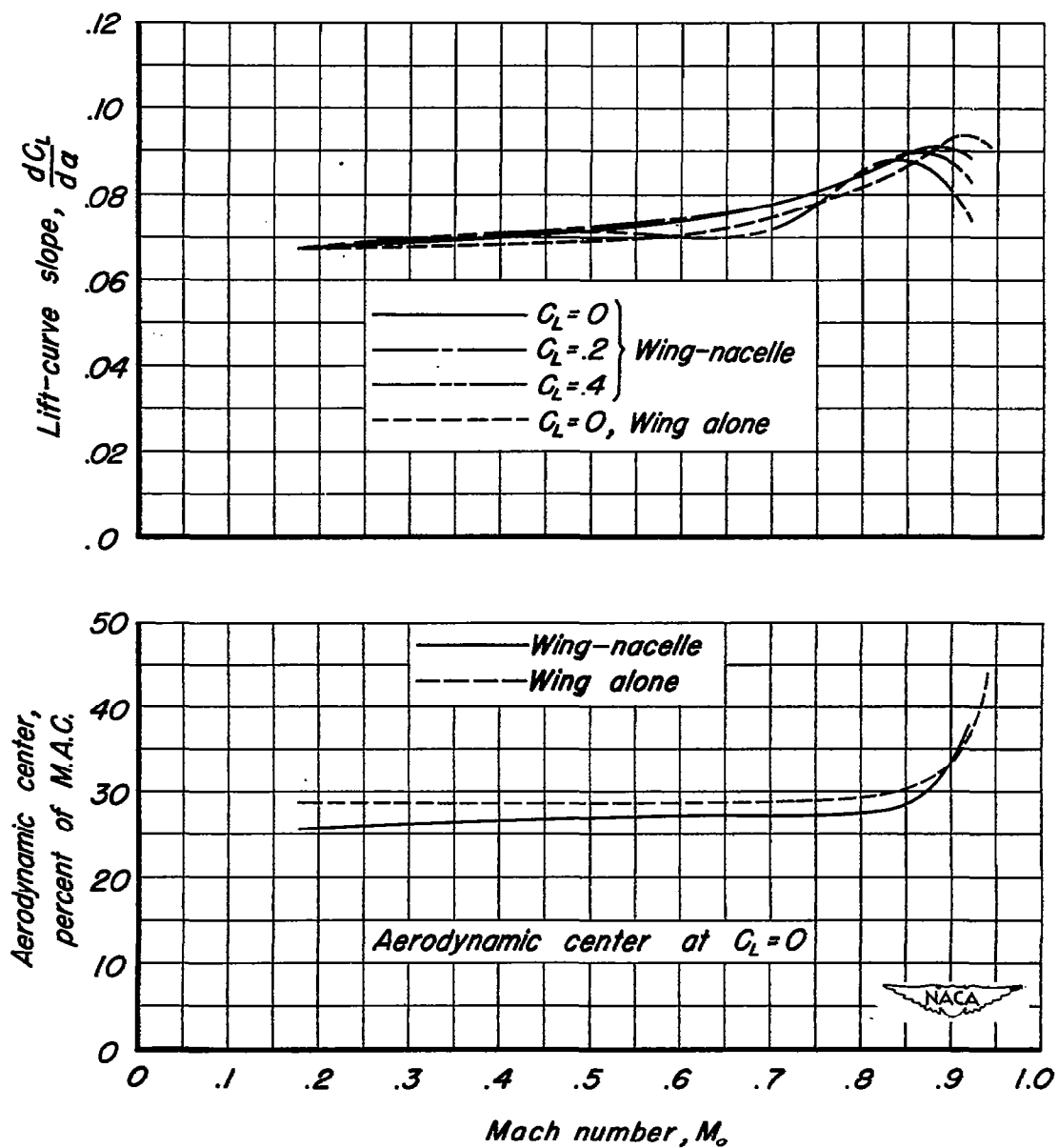
Figure 14.—The variation with Mach number of the lift-curve slope and the aerodynamic center.
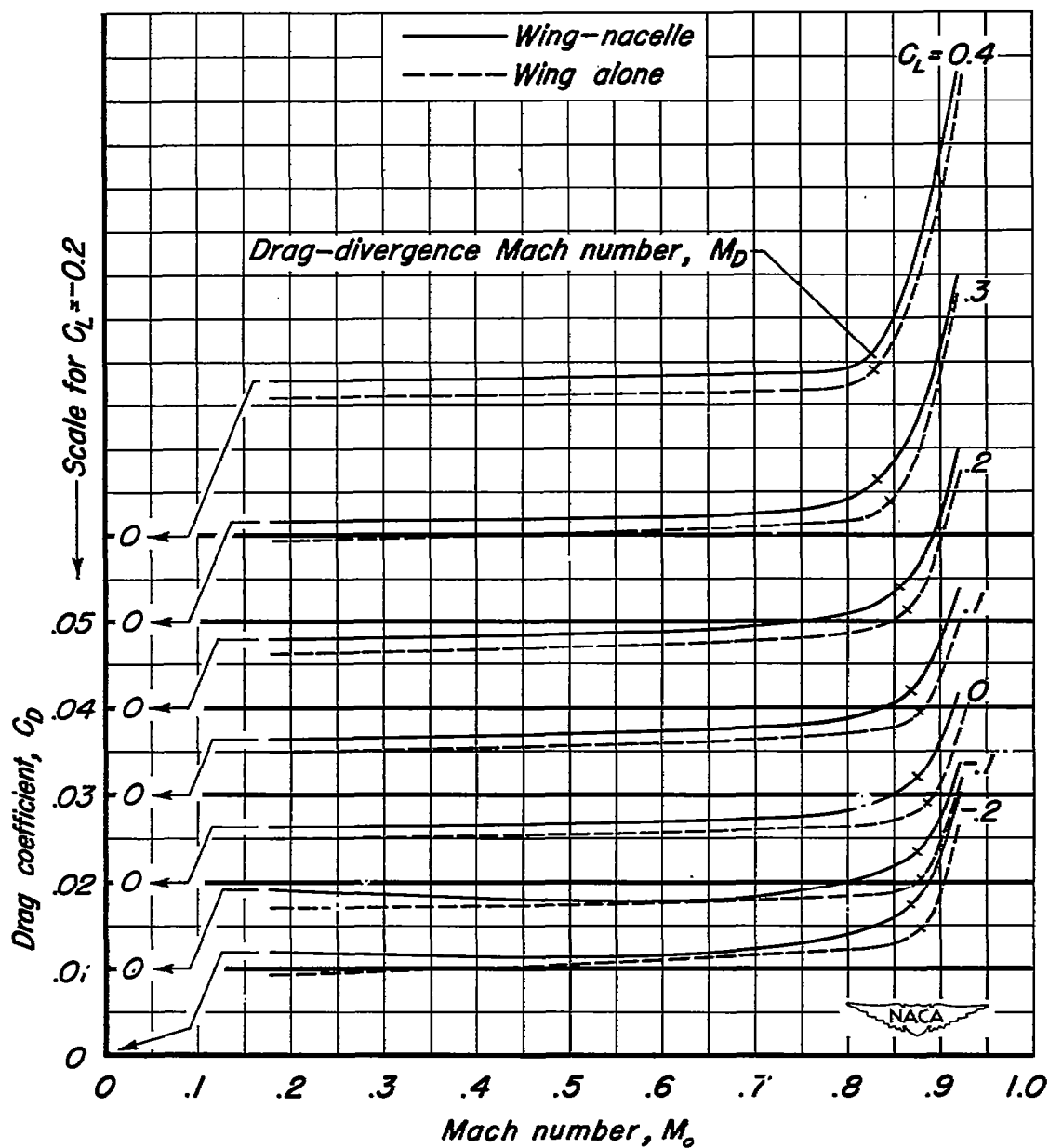
Figure 15.-The variation with Mach number of the drag coefficient at several values of lift coefficient.
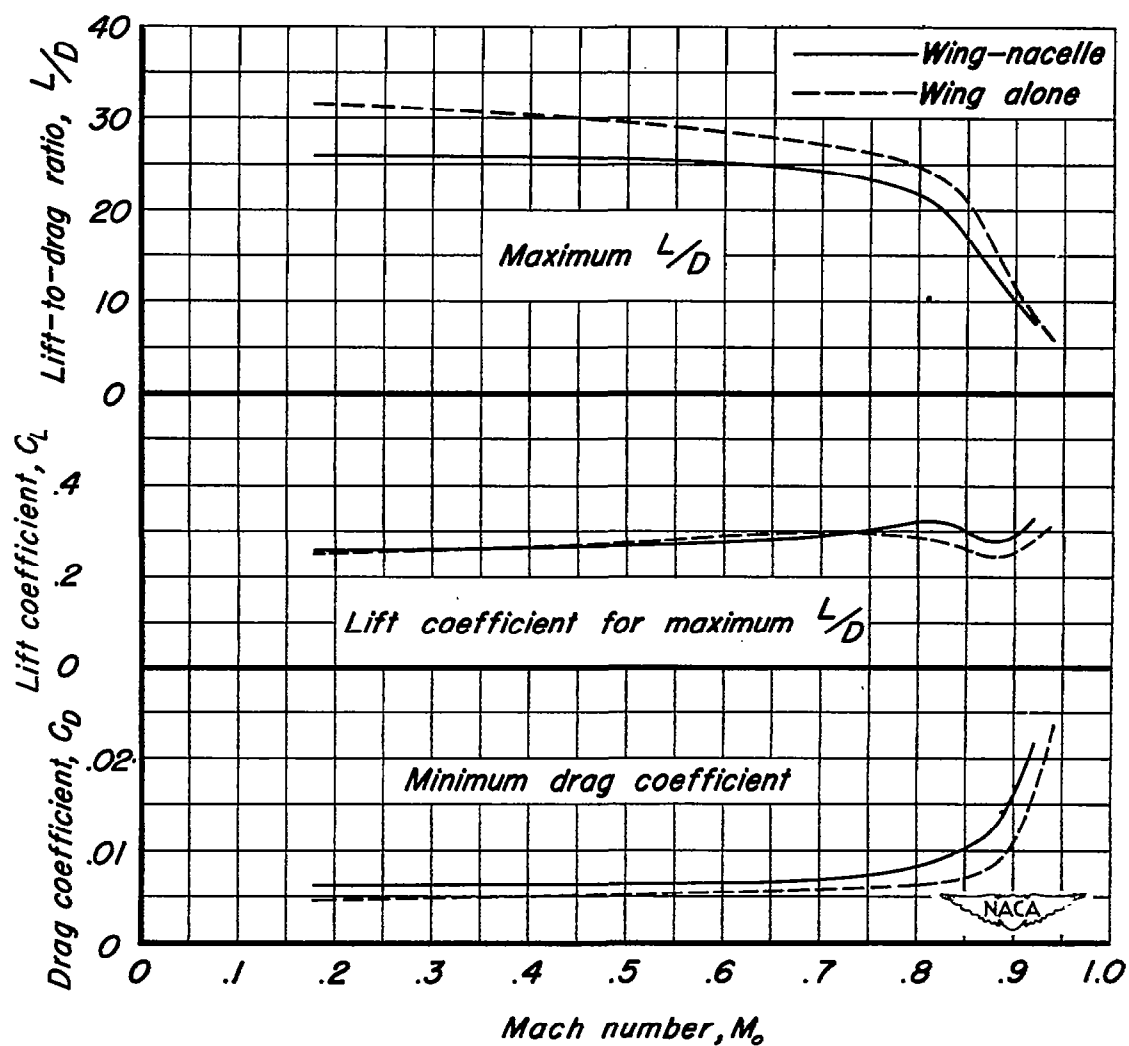
Figure 16.—The variation with Mach number of the maximum lift-to-drag ratio, the lift coefficient for maximum lift-to-drag ratio, and the minimum drag coefficient.

Line of constant
pressure coefficient

Crest line

$M_o = 0.18$
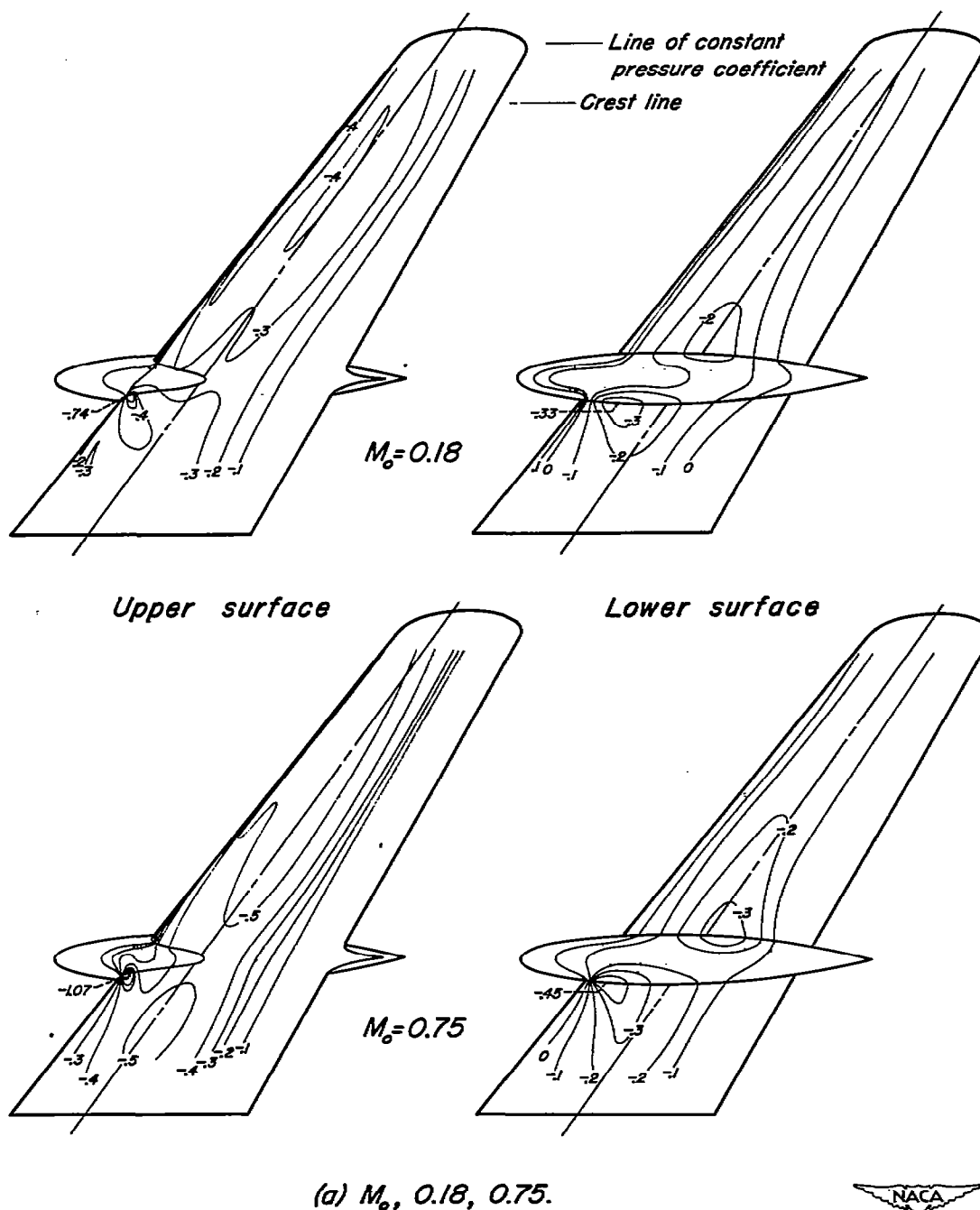
Upper surface

Lower surface

$M_o = 0.75$

(a) M_o, 0.18, 0.75.
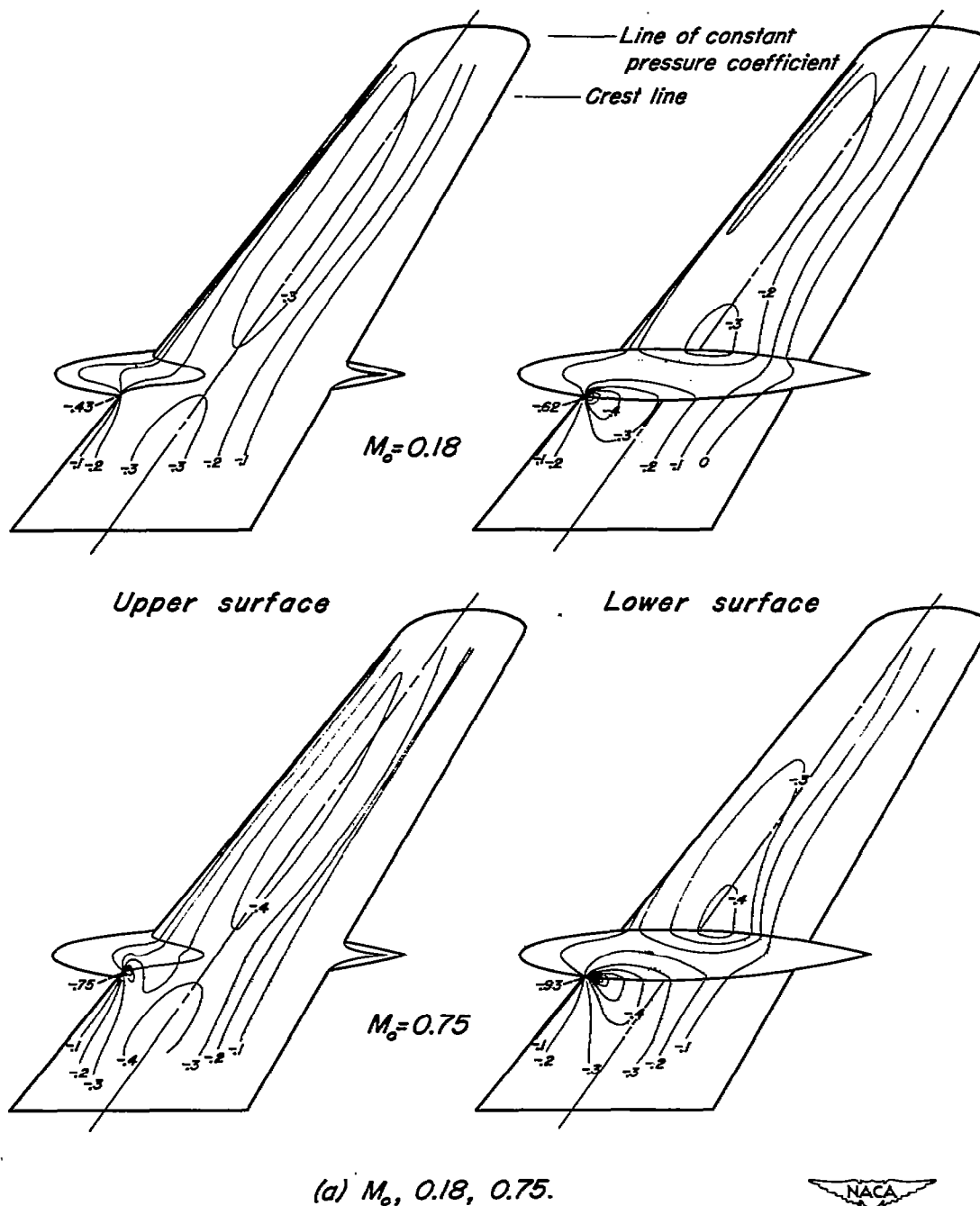
Figure 17.-The lines of constant pressure coefficient on the upper and lower
surfaces for several Mach numbers. a_u, 0°; R_w, 2,000,000.

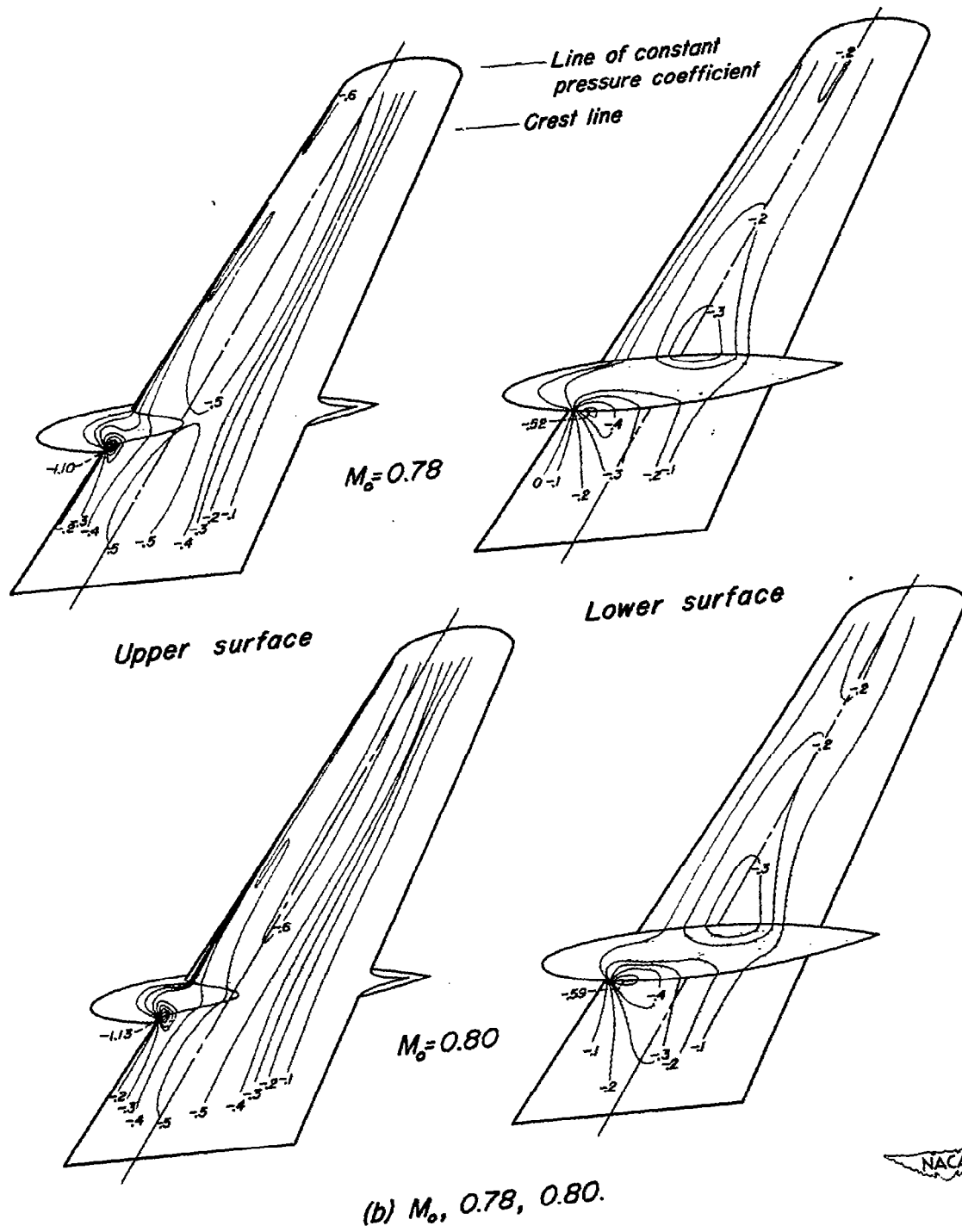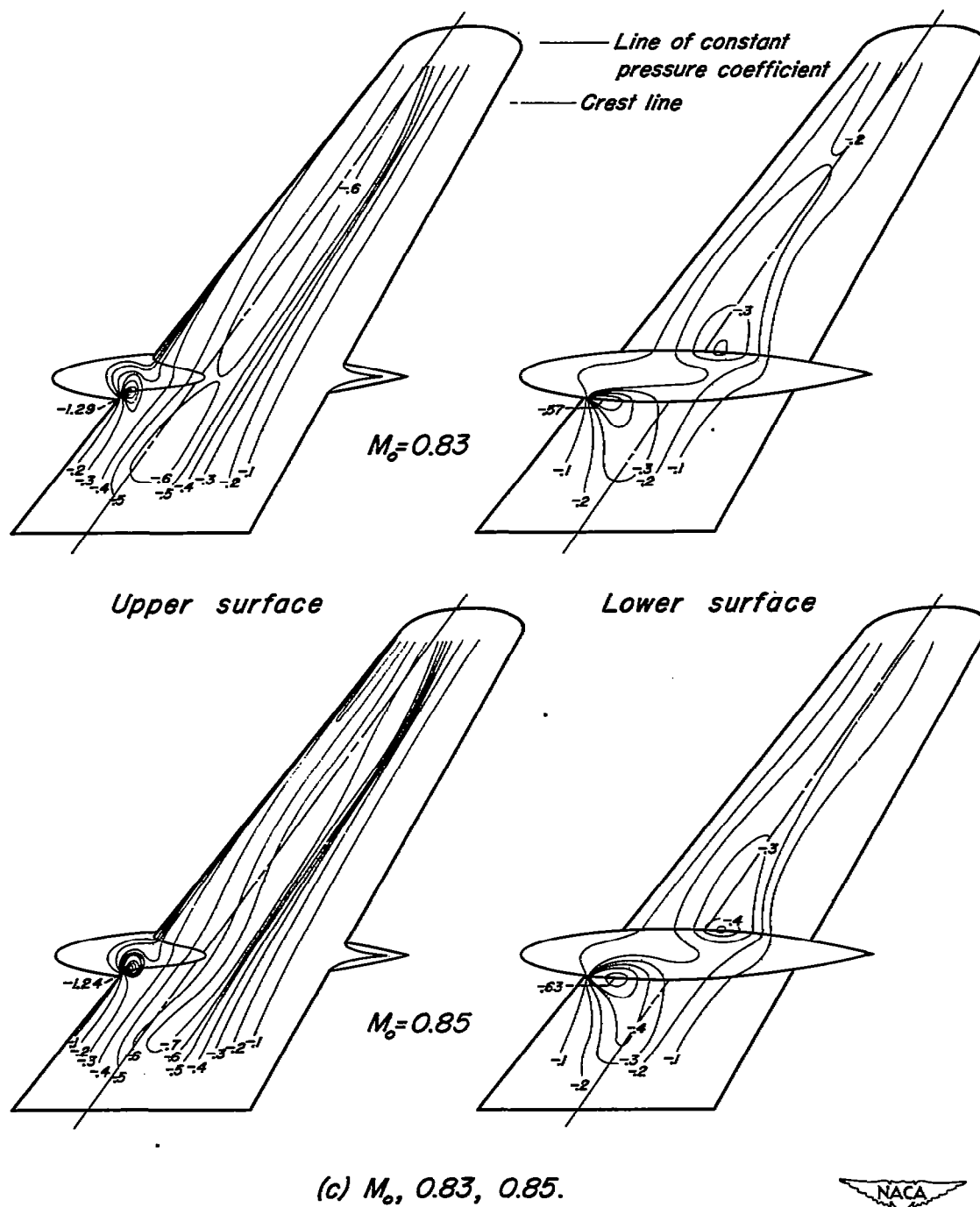Line of constant
pressure coefficient

Crest line

$M_o = 0.78$

Upper surface

Lower surface

$M_o = 0.90$

(b) M_o, 0.78, 0.80.

Figure 17.-Continued.

Line of constant
pressure coefficient
Crest line

$M_o = 0.83$

Upper surface   Lower surface

$M_o = 0.85$

(c) M_o, 0.83, 0.85.

Figure 17.-Continued.

Line of constant
pressure coefficient

Crest line

$M_o = 0.88$

Upper surface   Lower surface

$M_o = 0.90$

(d) M_o, 0.88, 0.90.
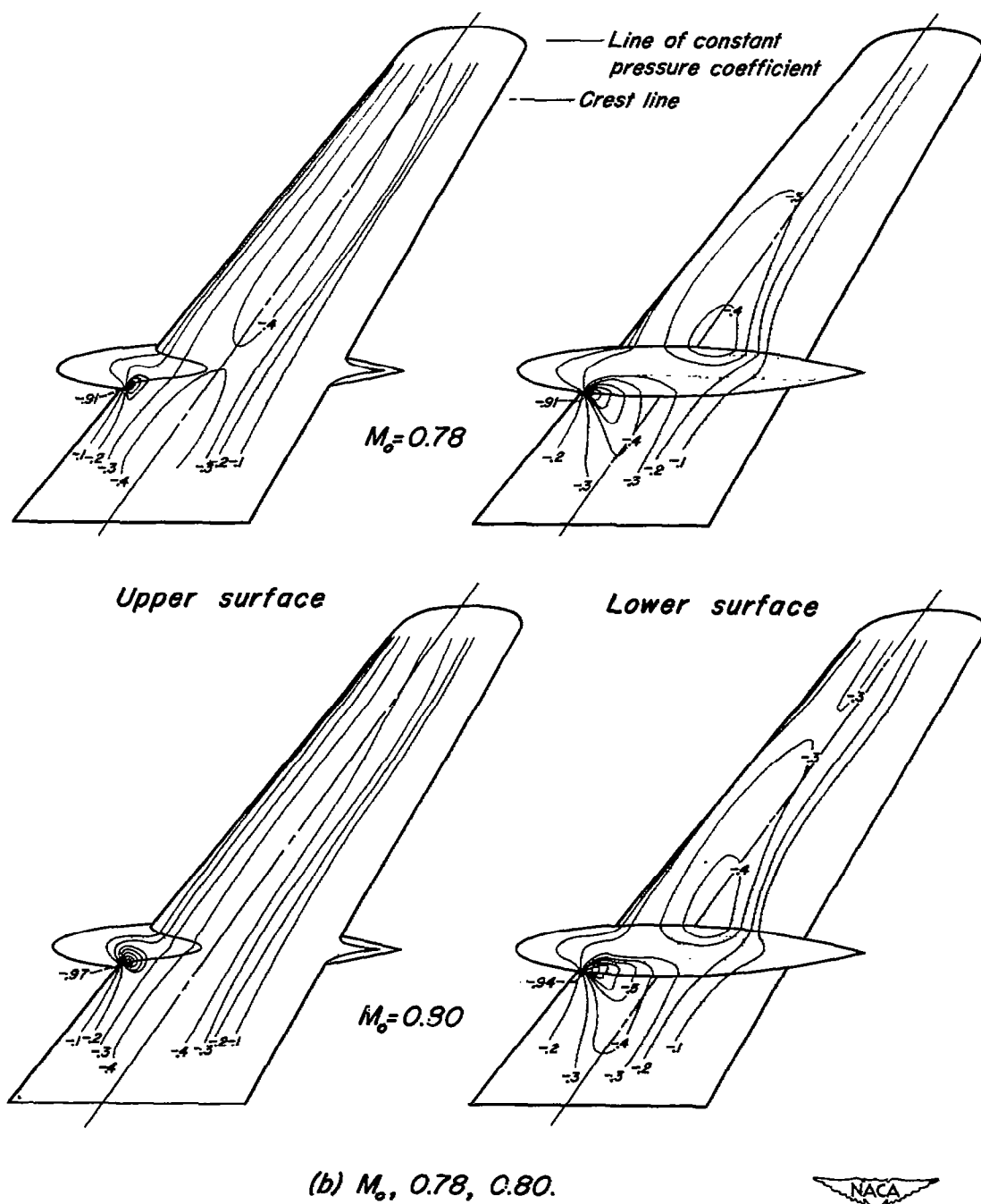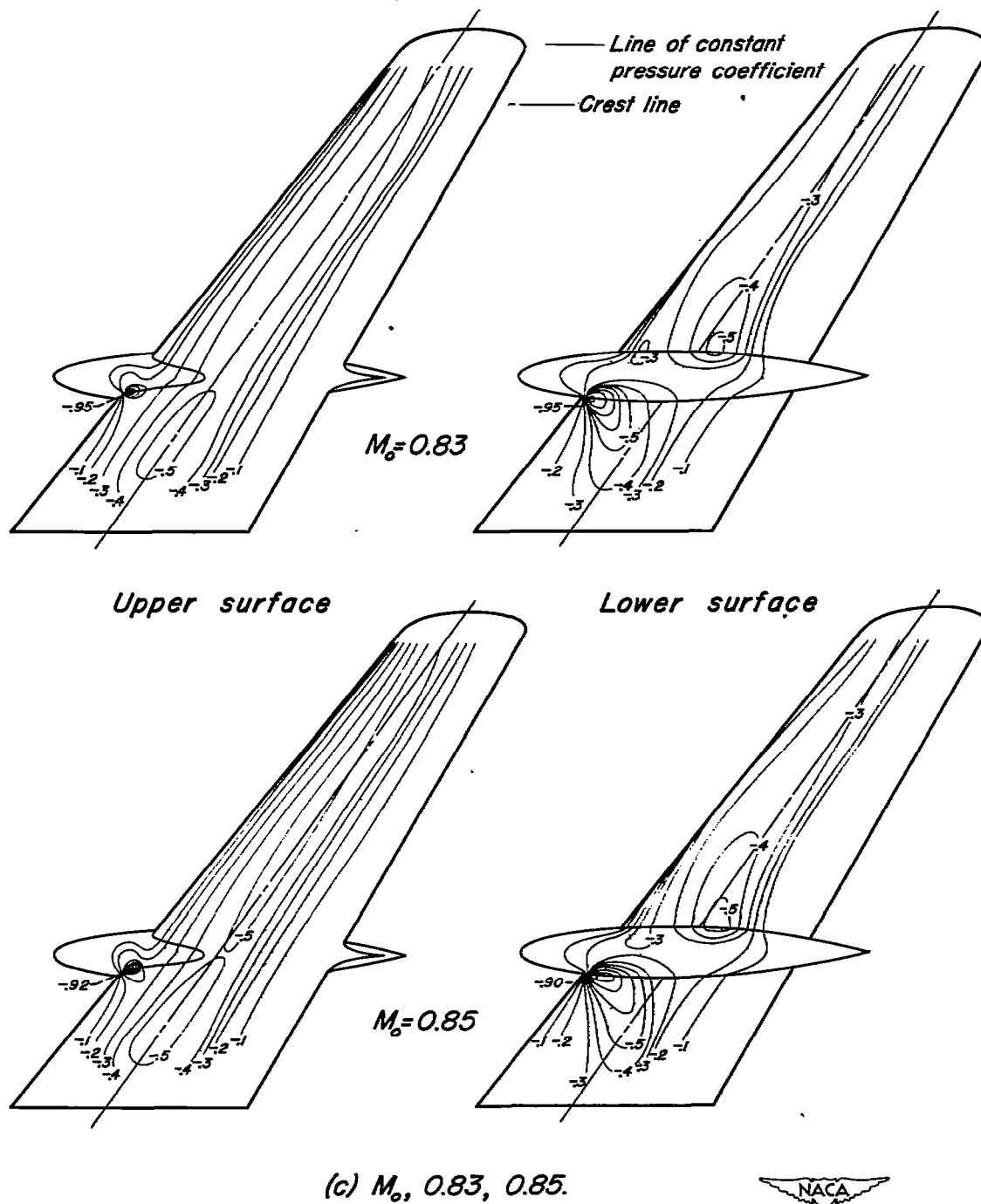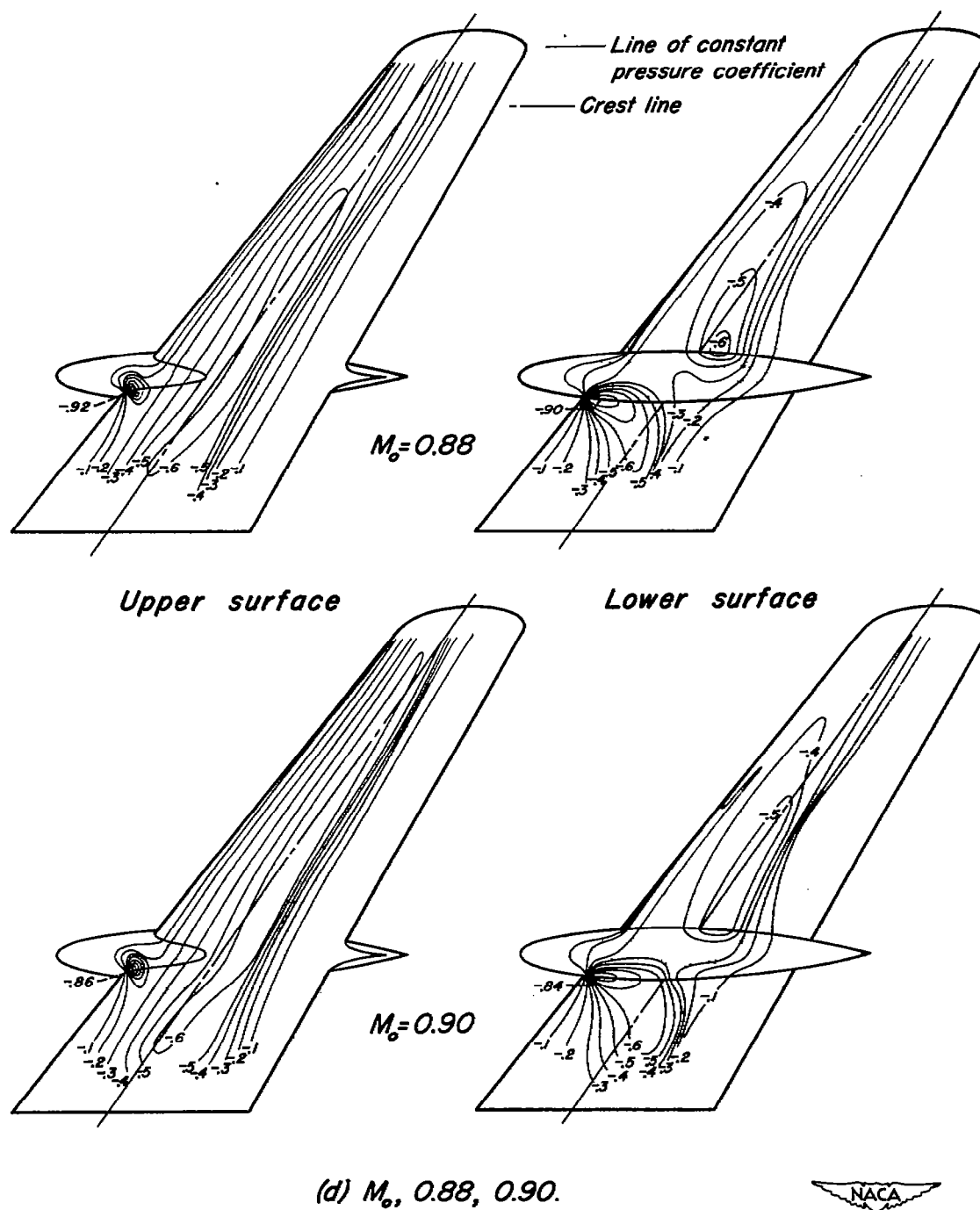
Figure 17.-Concluded.

(a) M_o, 0.18, 0.75.
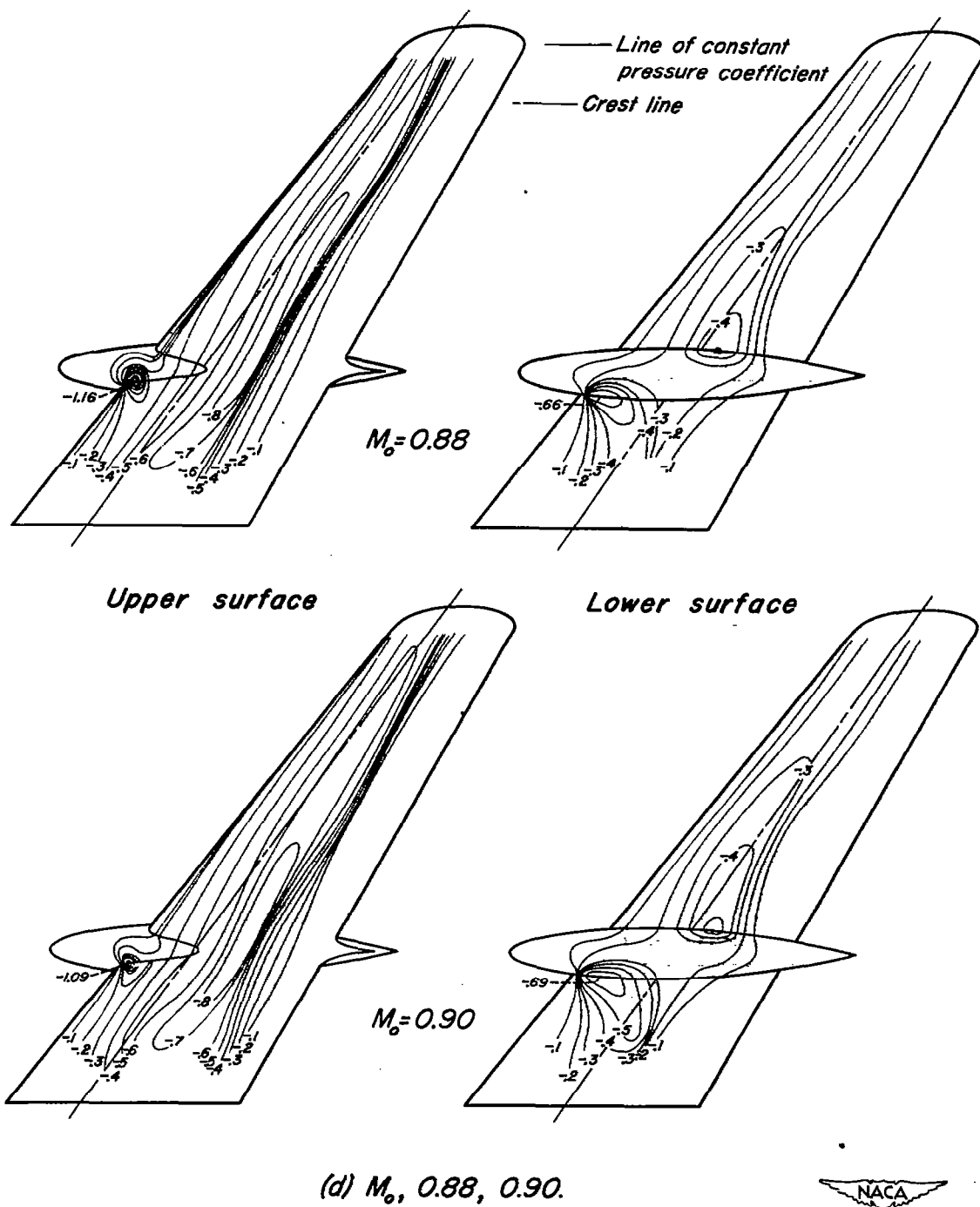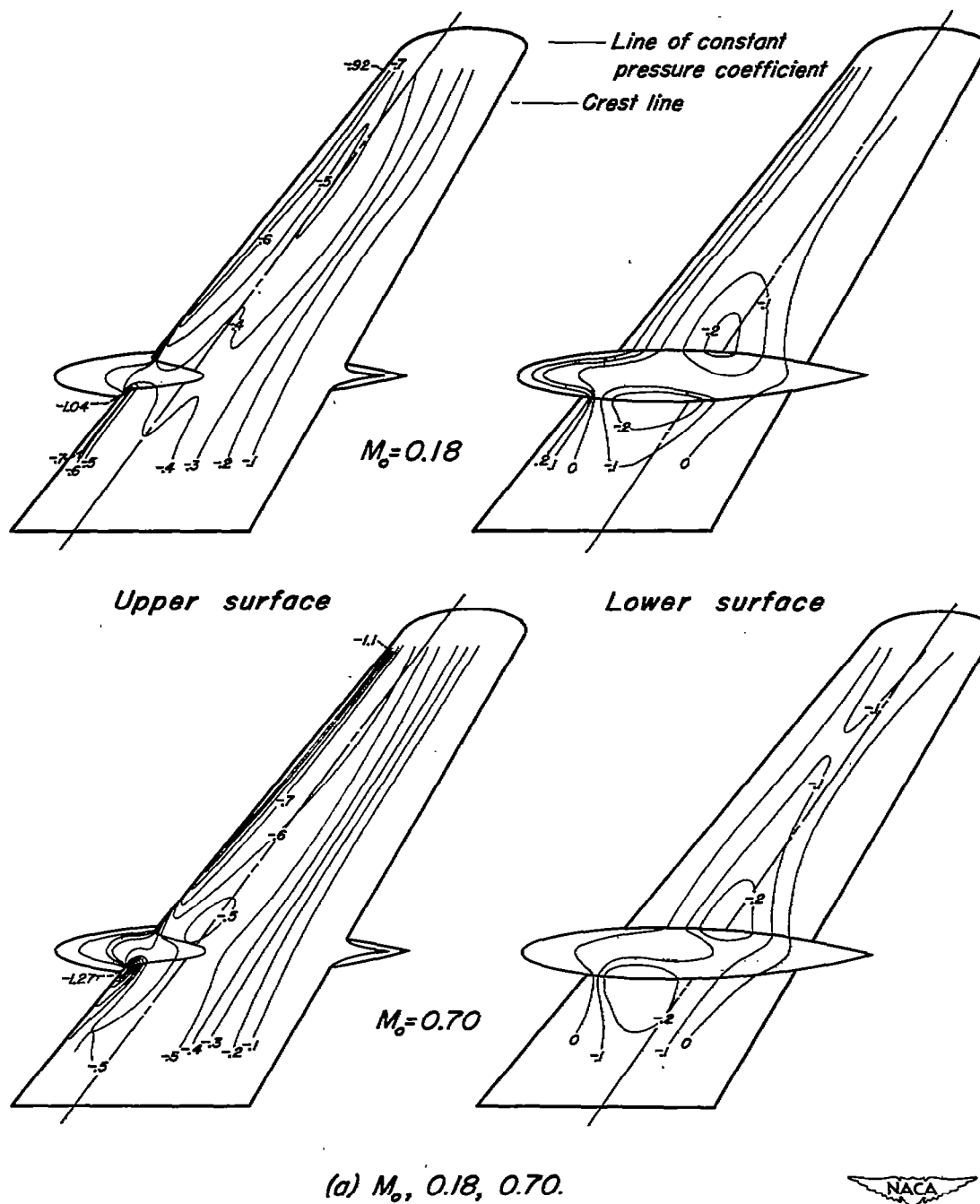
Figure 18.–The lines of constant pressure coefficient on the upper and lower surfaces for several Mach numbers. a_u, 2°; R_w, 2,000,000.
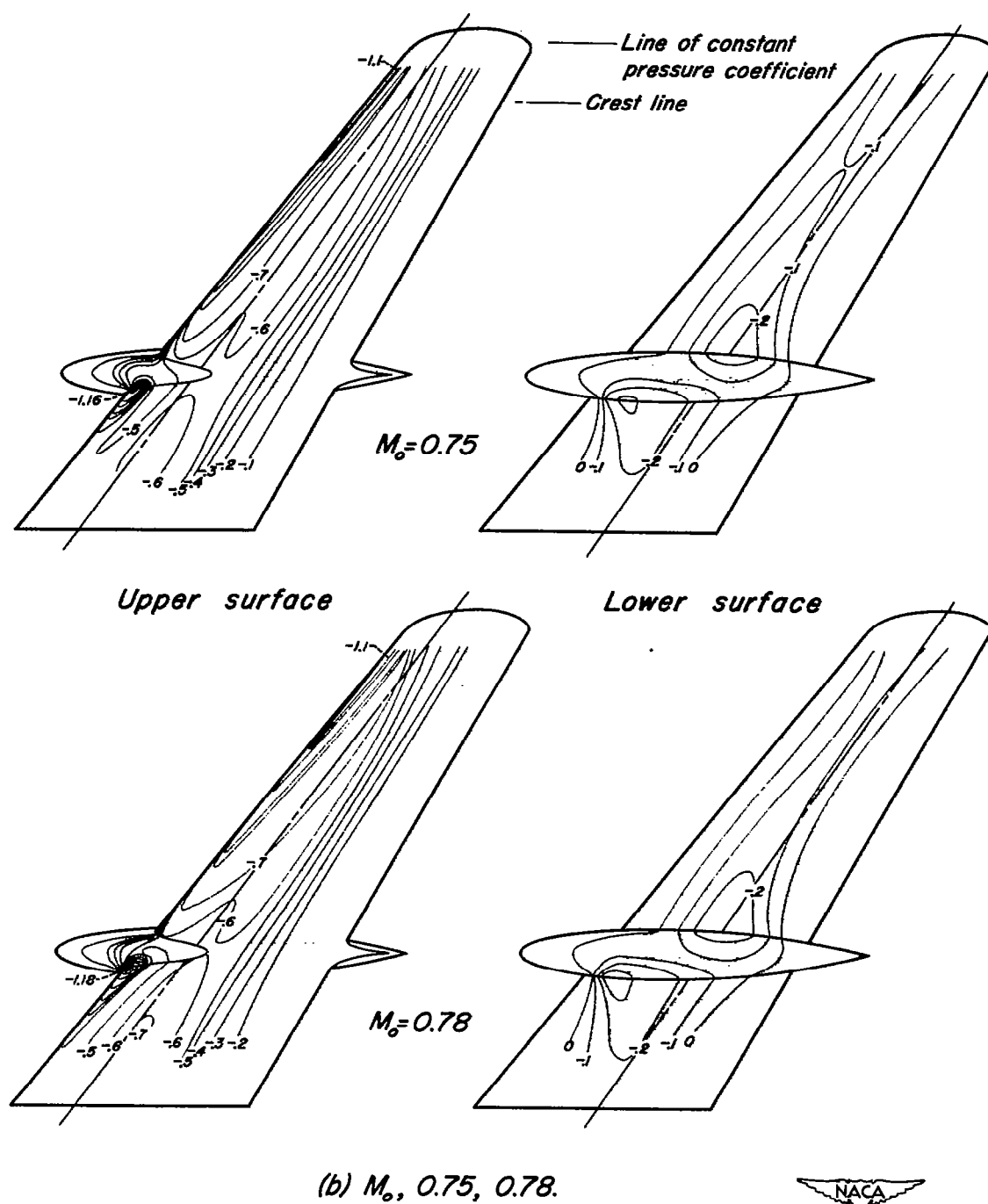
Line of constant
pressure coefficient
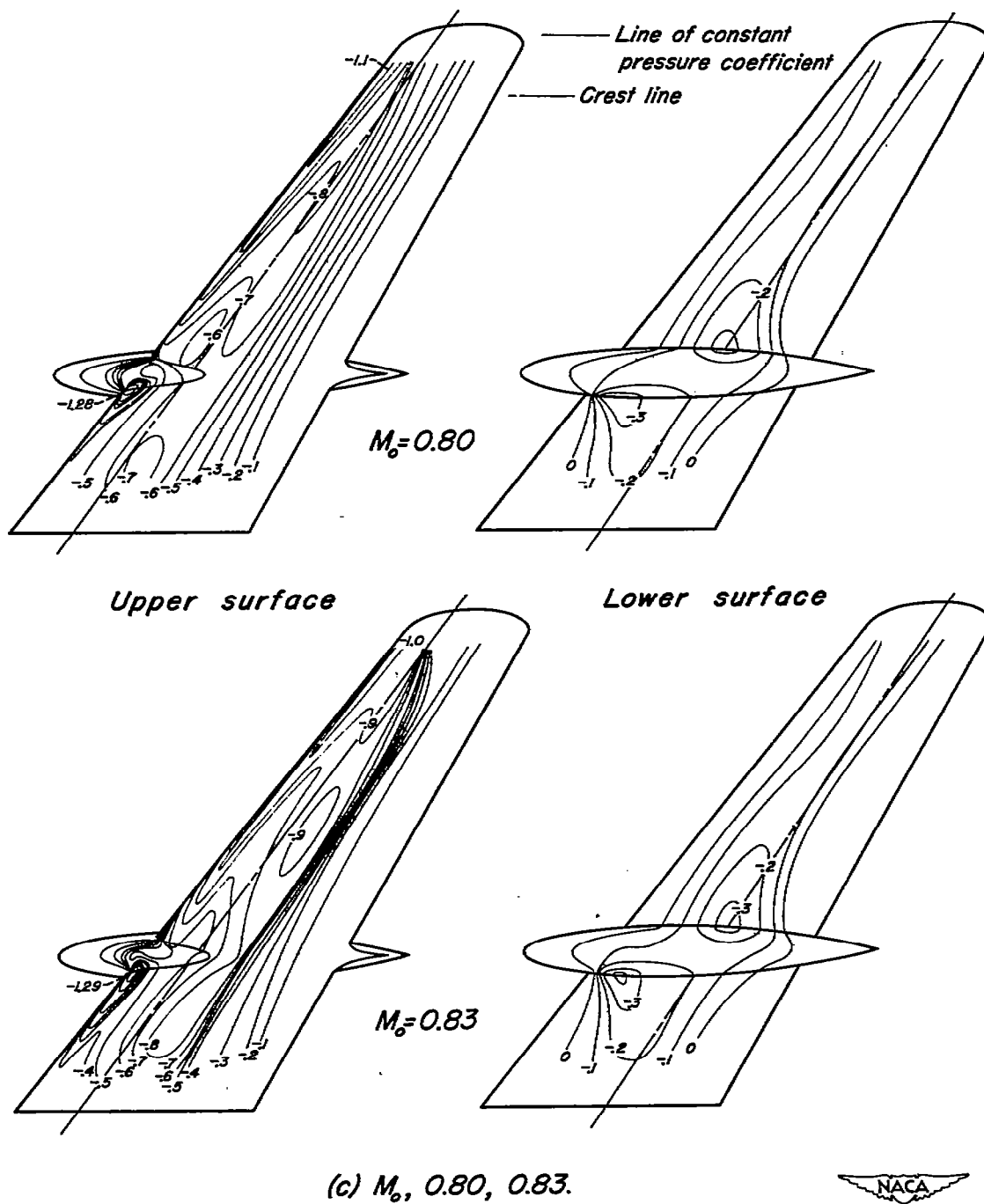
Crest line

$M_0 = 0.78$

Upper surface

Lower surface

$M_0 = 0.80$

(b) M_o, 0.78, 0.80.

Figure 18.-Continued.

Line of constant
pressure coefficient
------ Crest line

$M_o = 0.83$

Upper surface   Lower surface

$M_o = 0.85$

(c) M_o, 0.83, 0.85.

Figure 18.-Continued.

Line of constant pressure coefficient

Crest line

$M_o = 0.88$

Upper surface

Lower surface

$M_o = 0.90$

(d) M_o, 0.88, 0.90.

Figure 18.—Concluded.

Line of constant
pressure coefficient
Crest line

$M_o = 0.18$

Upper surface

Lower surface

$M_o = 0.70$

(a) M_o, 0.18, 0.70.

Figure 19.-The lines of constant pressure coèfficient on the upper and lower
surfaces for several Mach numbers. a_u, 4°; R_w, 2,000,000.

Upper surface   Lower surface

$M_o = 0.75$

$M_o = 0.78$

(b) M_o, 0.75, 0.78.

Figure 19.-Continued.

Line of constant
pressure coefficient
--- Crest line

$M_o = 0.80$

Upper surface   Lower surface

$M_o = 0.83$

(c) M_o, 0.80, 0.83.

Figure 19.-Continued.

Line of constant
pressure coefficient

Crest line

$M_o = 0.85$

Upper surface   Lower surface
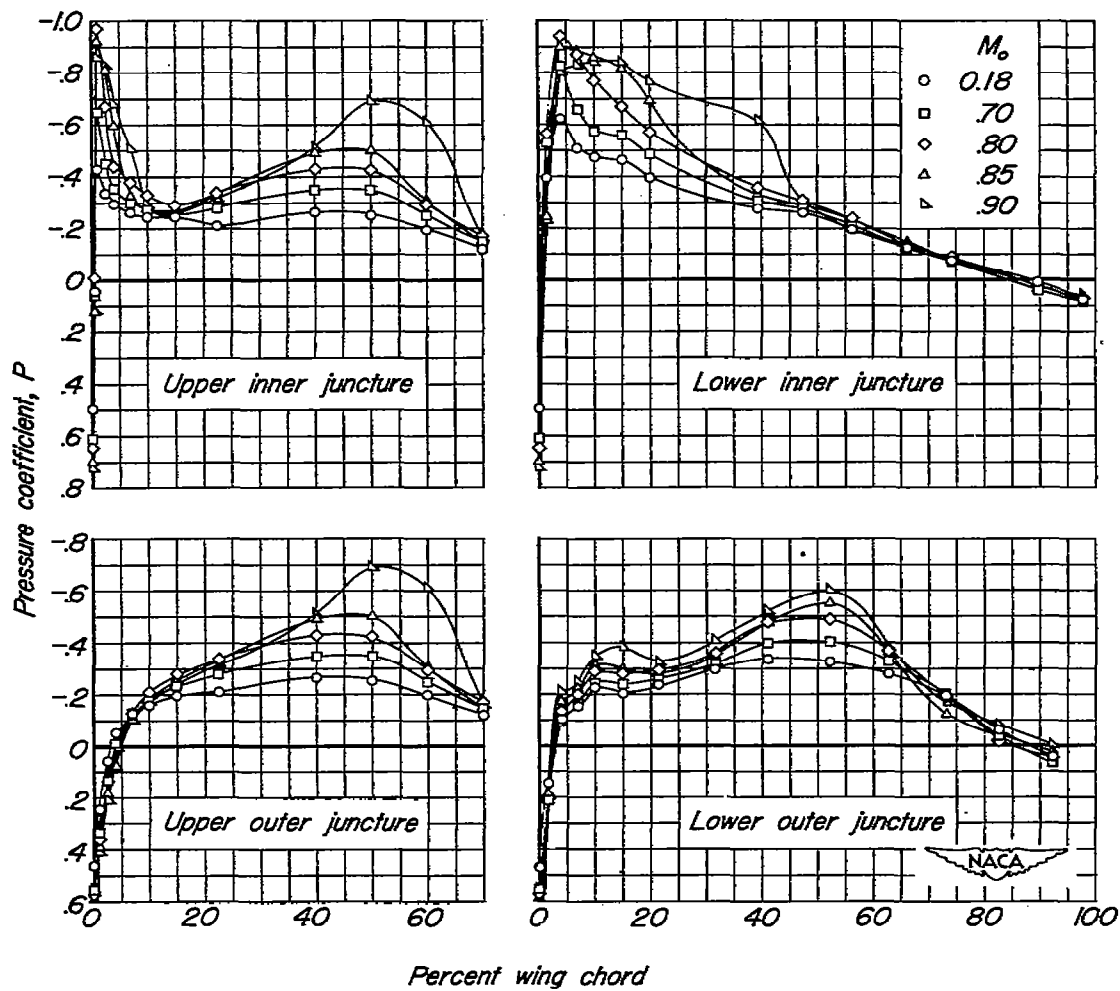
$M_o = 0.88$

(d) M_o, 0.85, 0.88.
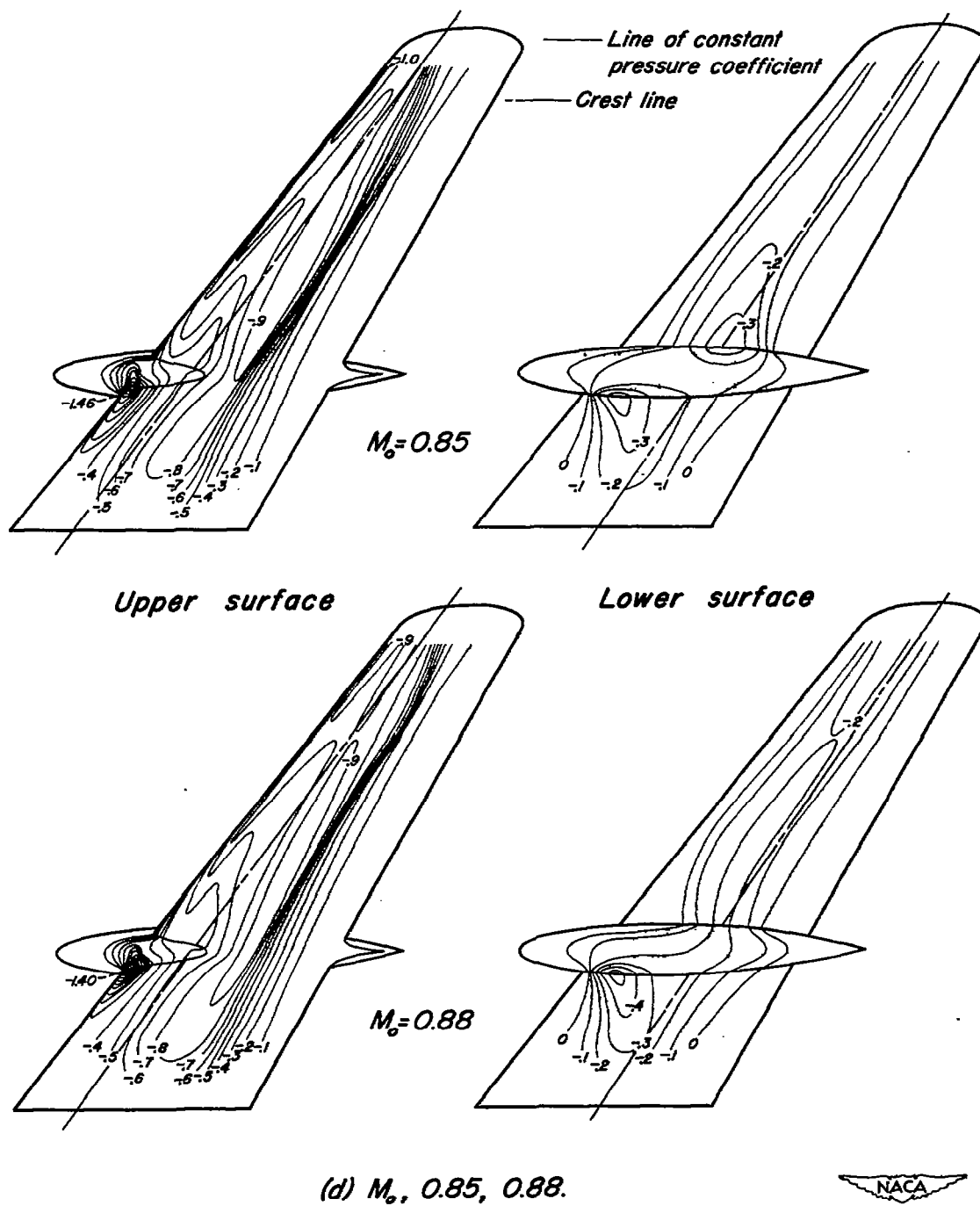
Figure 19.- Concluded.
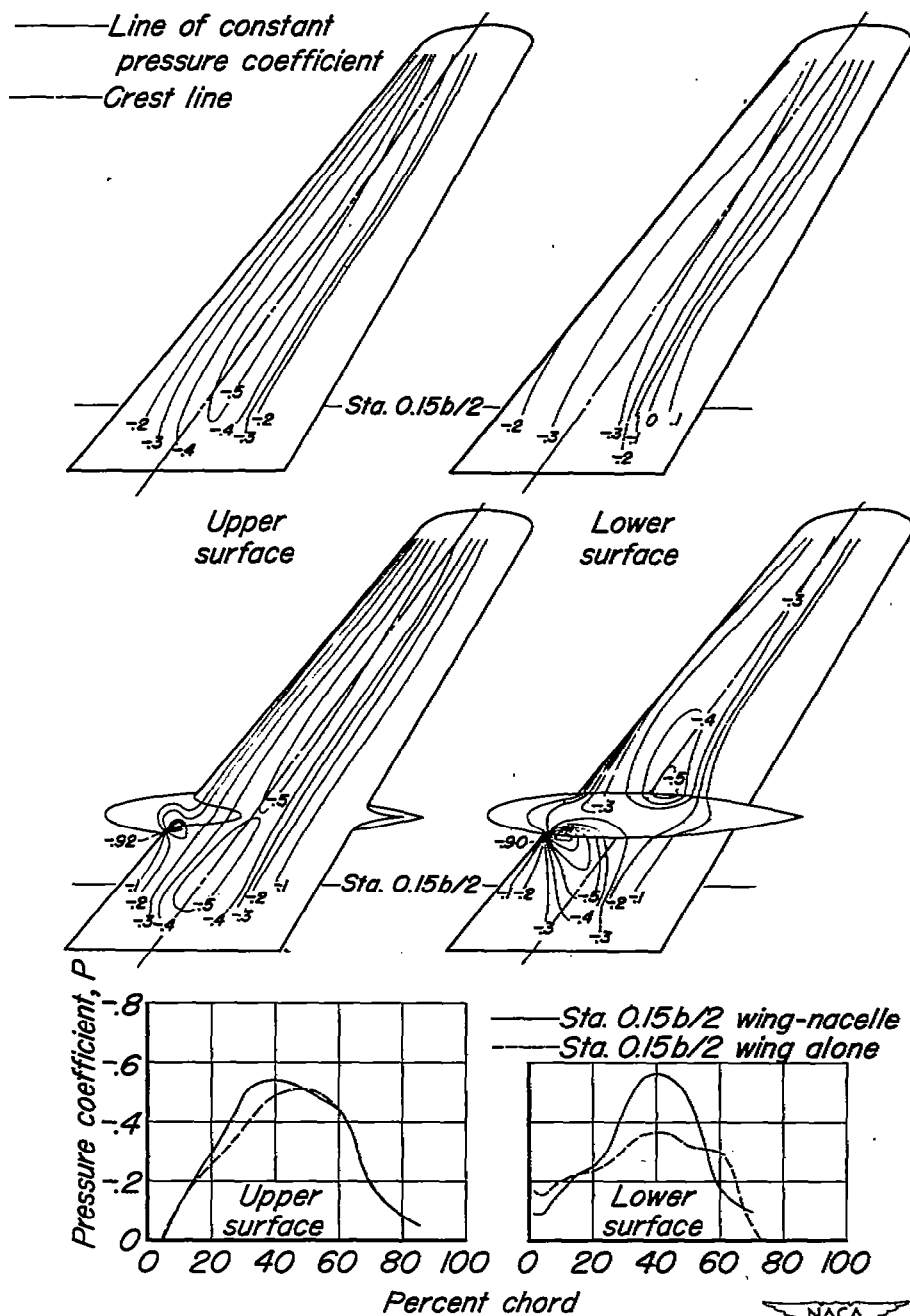
(a) a_u, $0°$; M_o, 0.85.

Figure 20.-A comparison of the pressures on the wing alone with those on the wing-nacelle combination. R_w, 2,000,000.

—— Line of constant
        pressure coefficient
——·—— Crest line

-1.0

-.9

-.8

-.7

-.6 -.5 -.2 -.3 -.4 -.5 -.2 -Sta. 0.15 b/2—

.2 0 -.1 -.1 0 -.1

Upper
surface

Lower
surface

-1.1

-.8

-1.28

-1.28

-.5 -.7 -.6 -.4 -.2 -Sta. 0.15 b/2—

-.6 -.5 -.3

0 -.2 -.1 0

-.2

-.3

0 -.2 -.1 0

$$\text{Pressure coefficient, } P$$

-.8
-.6
-.4
-.2
0
.2

Upper
surface

Lower
surface

—— Sta. 0.15 b/2 wing-nacelle
——·—— Sta. 0.15 b/2 wing alone

0   20 40 60 80 100   0   20 40 60 80 100

Percent chord

NACA
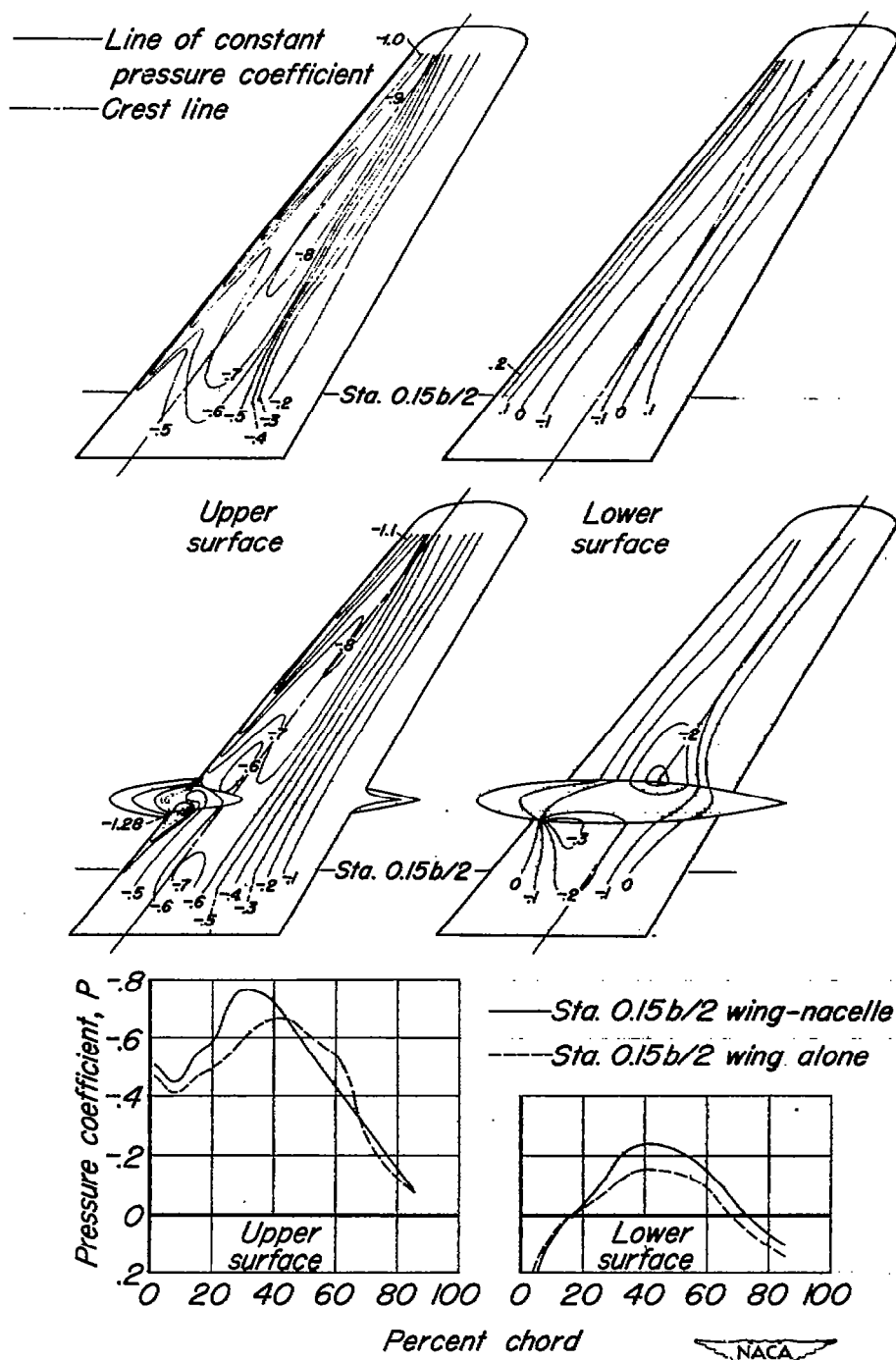
(b) a_u, 4°; M_o, 0.80.

Figure 20.-Concluded.

(a) a_u, $O°$.

Figure 21.—The chordwise distribution of pressure coefficient in the wing-nacelle junctures at several Mach numbers for three angles of attack. R_w, 2,000,000.
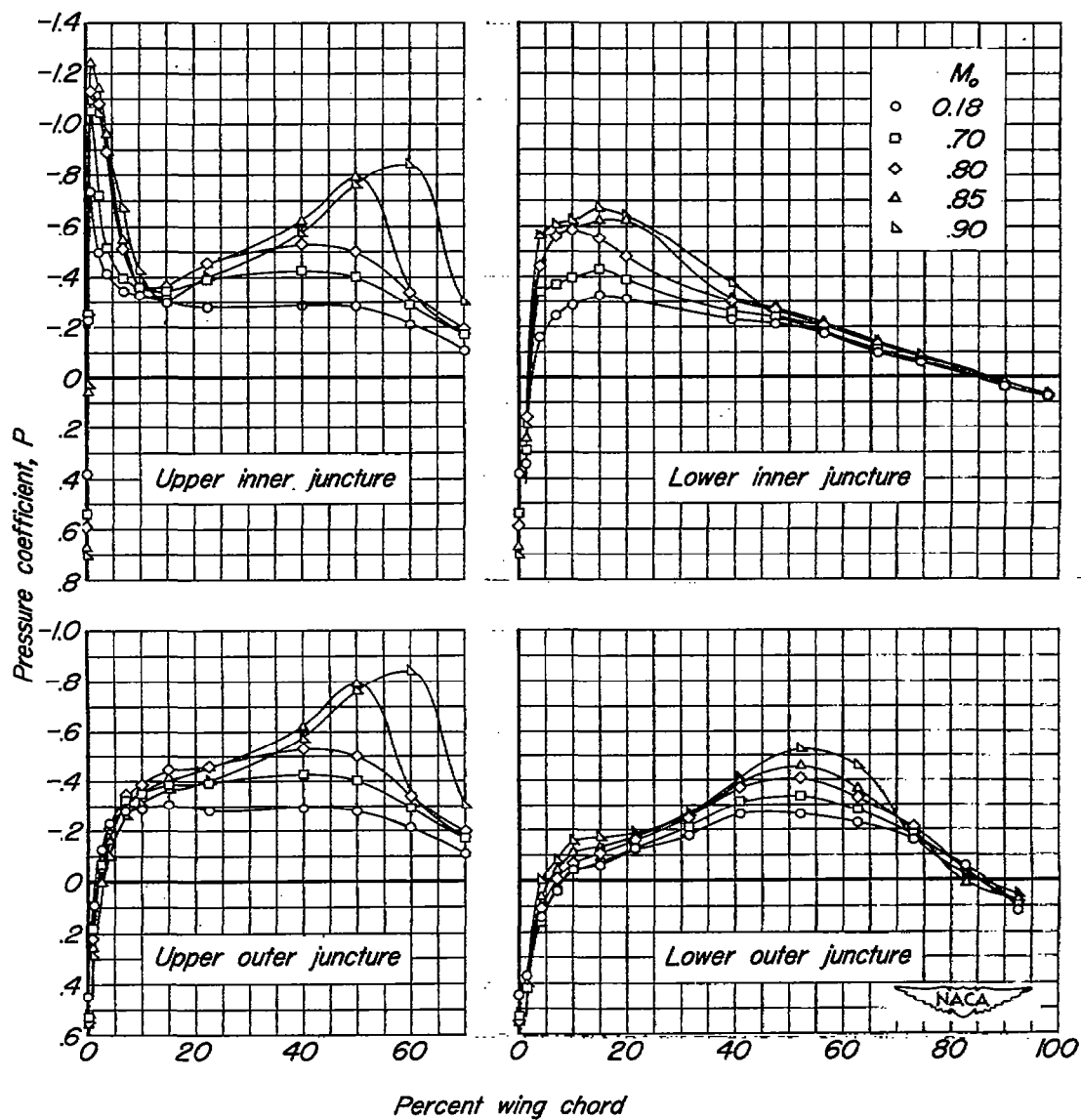
(b) a_u, 2°.

Figure 21.-Continued.
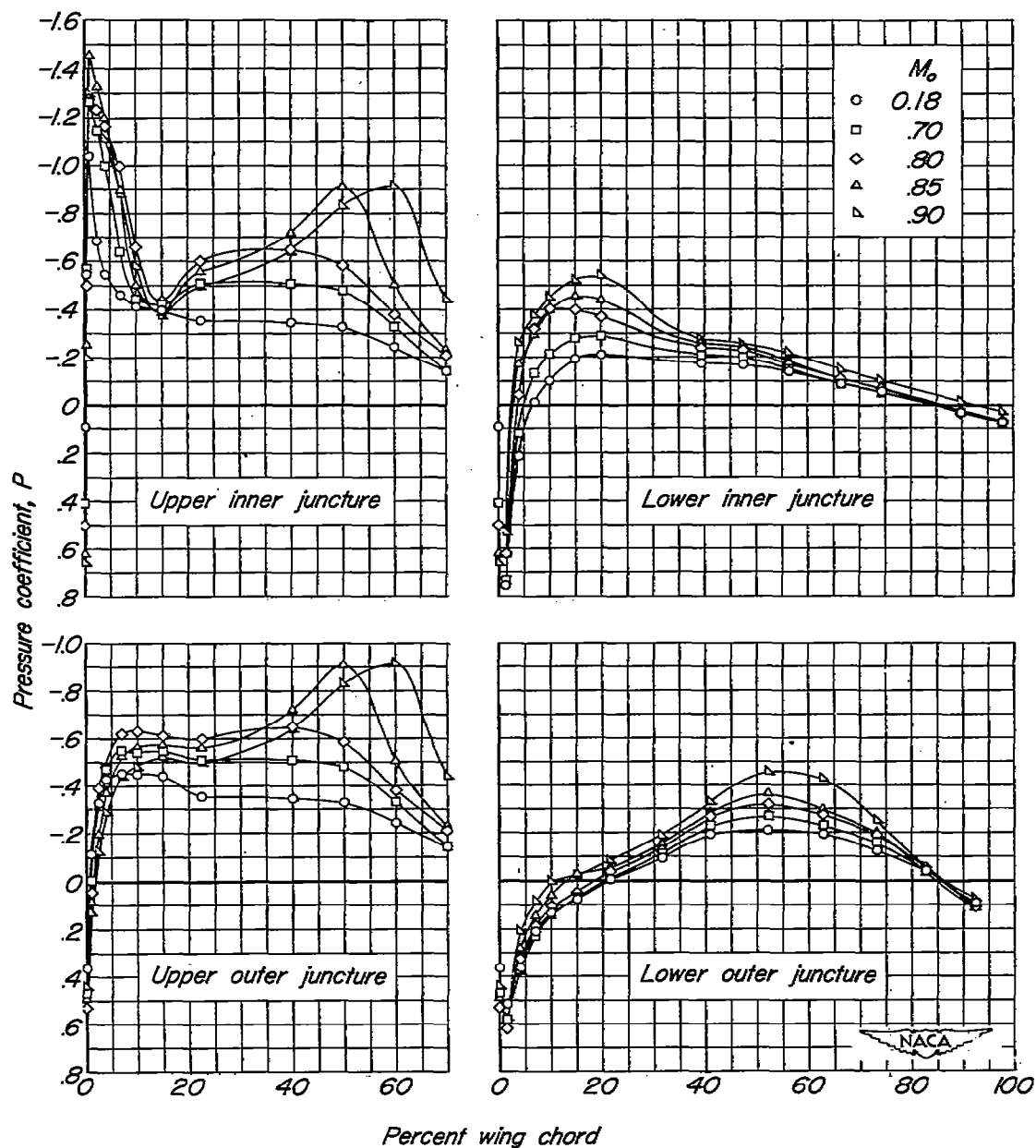
(c) a_u , *4°.*
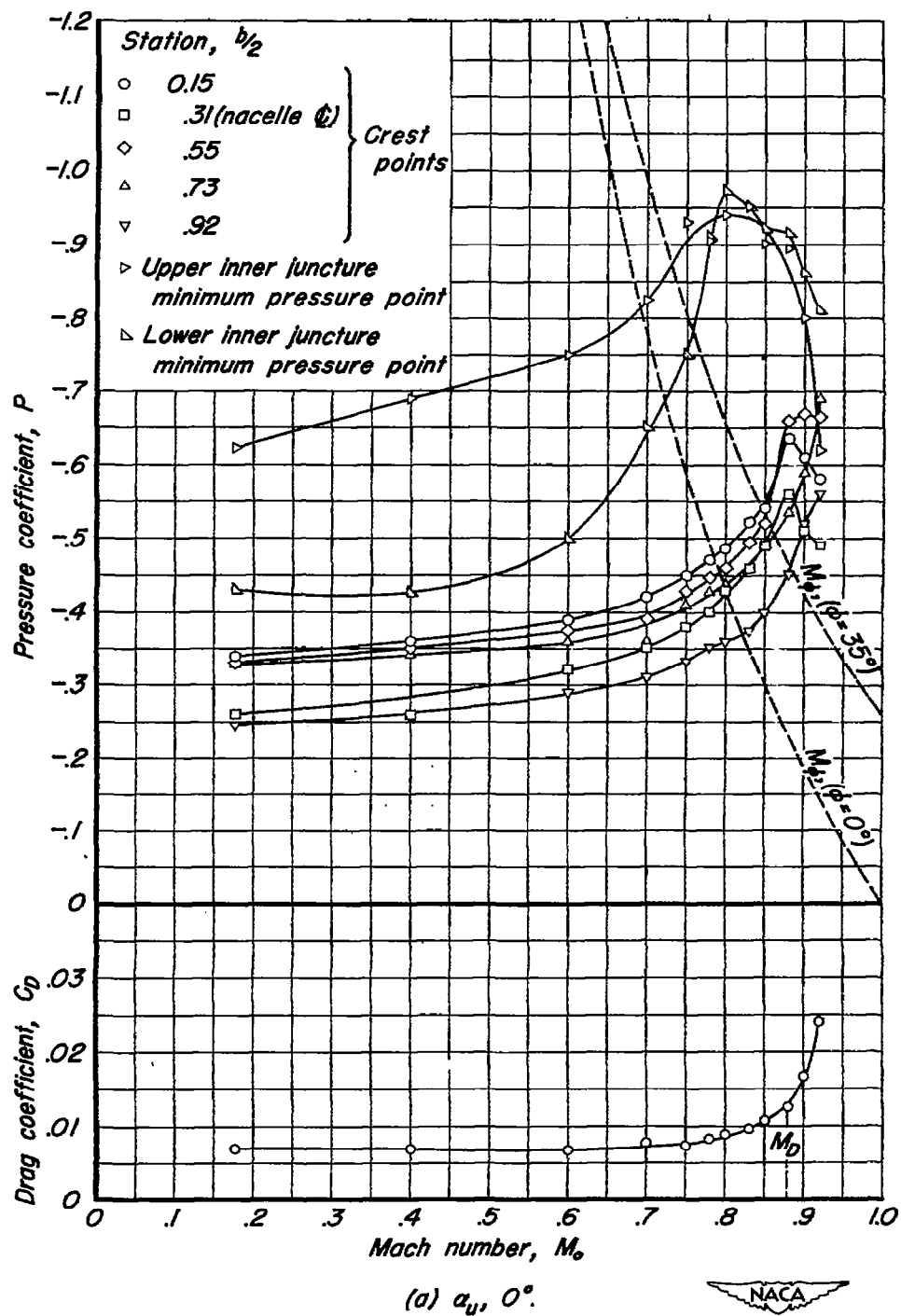
Figure 21.-Concluded.

Figure 22.—The variation with Mach number of the drag coefficient and of the pressure coefficients at several points on the wing-nacelle combination.
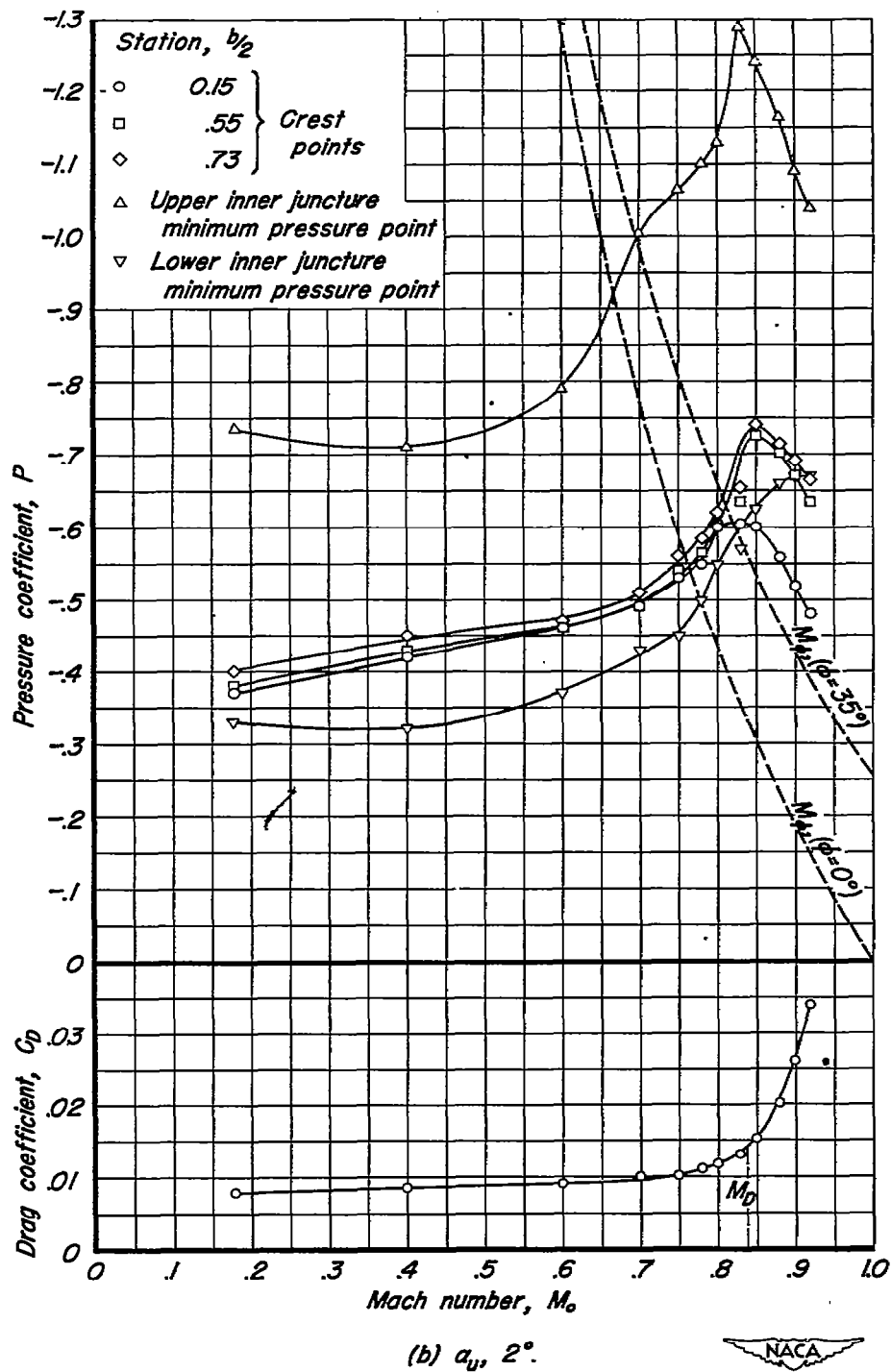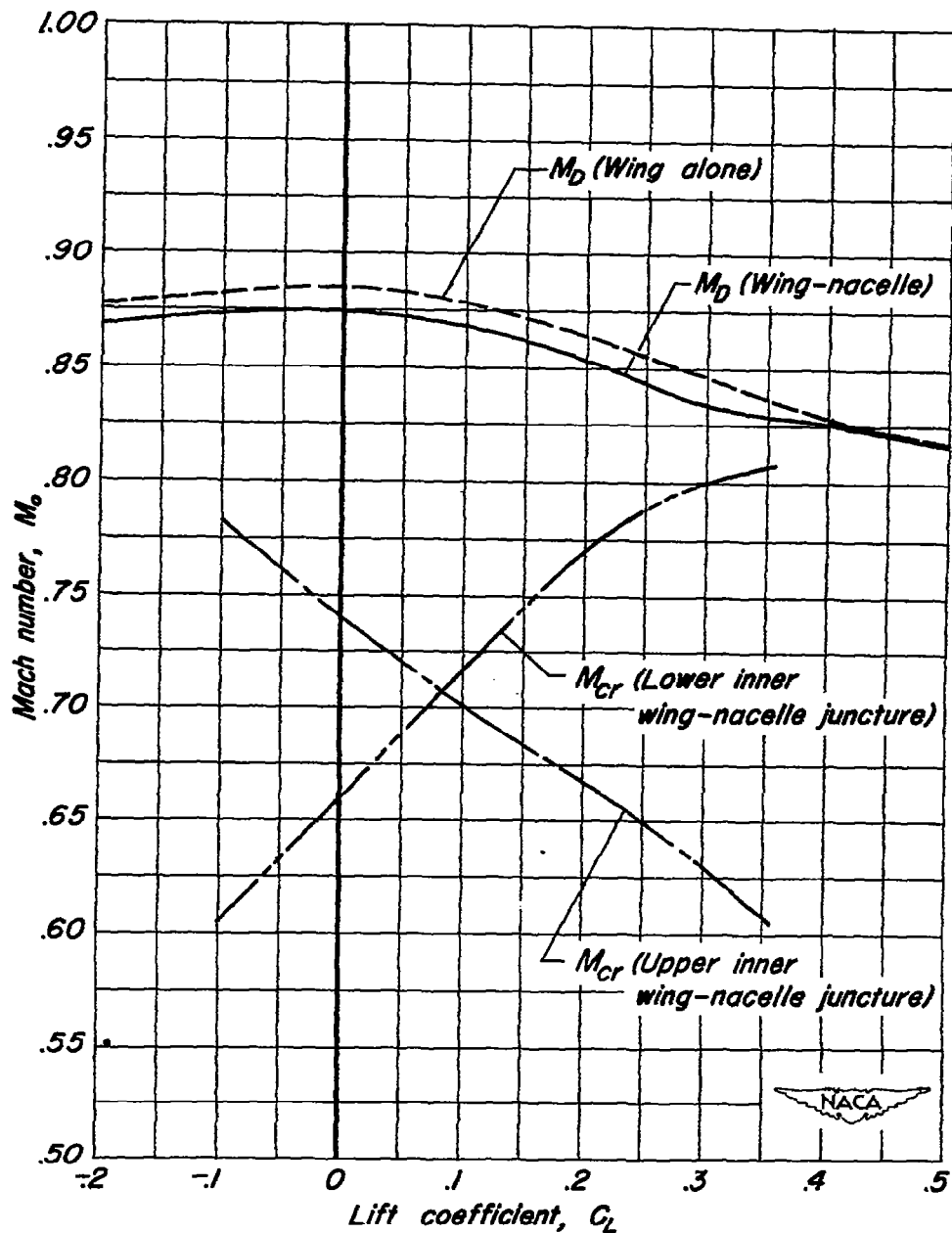
(b) a_u, 2°.

Figure 22.- Concluded.

Figure 23.—The variation with lift coefficient of the drag-divergence Mach number and the critical Mach numbers in the wing-nacelle junctures.